AD-A097 392 WESTINGHOUSE RESEARCH AND DEVELOPMENT CENTER PITTSBU--ETC F/G 13/8
INVESTIGATION OF WELD POOL STRUCTURE AND PROPERTY CONTROL IN PU--ETC(U)
MAR 80 G M ECER, G G LESSMANN, H D BRODY N00014-77-C-0596
UNCLASSIFIED 81-9D4-PULSE-R1 NL

1 OF 2
AD A
097392

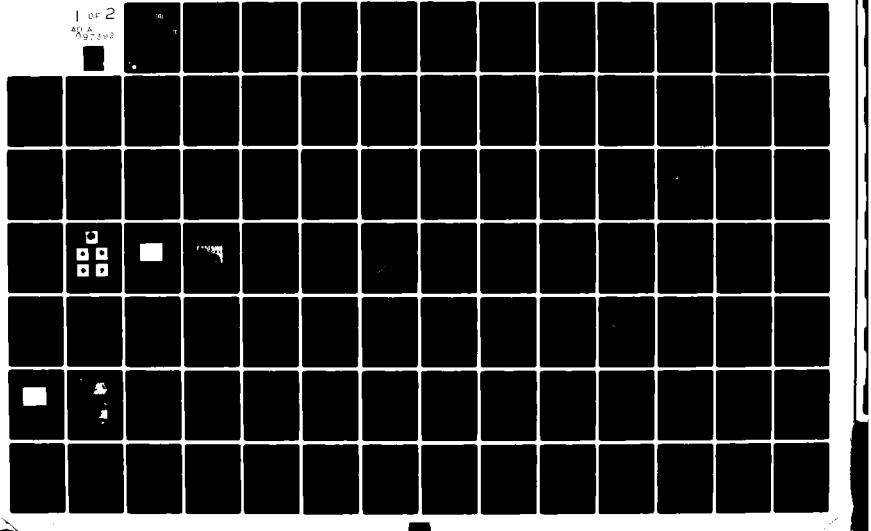

INVESTIGATION OF WELD POOL STRUCTURE AND PROPERTY CONTROL IN PULSED ARC WELDING

G. M. Ecer, Principal Investigator
G. G. Lessmann, Project Manager
Westinghouse R&D Center
Pittsburgh, PA 15235

H. D. Brody, Project Director
University of Pittsburgh
Pittsburgh, PA

LEVEL III

AD A097392

Final Report (September 15, 1977, through September 14, 1980)

ONR CONTRACT N00014-77-C0596

March 4, 1981

Office of Naval Research
800 North Qunicy Road
Arlington, VA 22217

Scientific Officer: Bruce A. MacDonald (Code 471)

Westinghouse R&D Center
1310 Beulah Road
Pittsburgh, Pennsylvania 15235

SECURITY CLASSIFICATION OF THIS PAGE (When Data Entered)

REPORT DOCUMENTATION PAGE

READ INSTRUCTIONS BEFORE COMPLETING FORM

1. REPORT NUMBER	2. GOVT ACCESSION NO. AD-A097392
3. RECIPIENT'S CATALOG NUMBER	
4. TITLE (and Subtitle) INVESTIGATION OF WELD POOL STRUCTURE AND PROPERTY CONTROL IN PULSED ARC WELDING.	5. TYPE OF REPORT & PERIOD COVERED FINAL REPORT, Sept. 15, 1977 to Sept. 14, 1980
	6. PERFORMING ORG. REPORT NUMBER 15 Sep '77 - 14 Sep 80
7. AUTHOR(s) G. M. Ecer / G. G. Lessmann / H. D. Brody	8. CONTRACT OR GRANT NUMBER(s) N00014-77-C0596
9. PERFORMING ORGANIZATION NAME AND ADDRESS Westinghouse R&D Center, Pittsburgh, PA 15235 University of Pgh., MME Dept., Pgh., PA 15213	10. PROGRAM ELEMENT, PROJECT, TASK AREA & WORK UNIT NUMBERS 4 11 Mar 81
11. CONTROLLING OFFICE NAME AND ADDRESS Office of Naval Research Metallurgy and Ceramics Program Arlington, VA 22217	12. REPORT DATE March 4, 1980
	13. NUMBER OF PAGES 122
14. MONITORING AGENCY NAME & ADDRESS (if different from Controlling Office) Dr. B. A. MacDonald, Metallurgy Division Office of Naval Research, Code 471 Department of the Navy Arlington, VA 22217	15. SECURITY CLASS. (of this report) Unclassified
	15a. DECLASSIFICATION/DOWNGRADING SCHEDULE

16. DISTRIBUTION STATEMENT (of this Report)

81-924-PULSE TI

17. DISTRIBUTION STATEMENT (of the abstract entered in Block 20, if different from Report)

Approved for public release; distribution unlimited.

18. SUPPLEMENTARY NOTES

19. KEY WORDS (Continue on reverse side if necessary and identify by block number)

Structure, Solidification, Pulsed, Arcs, Welding, Control, Heat, Flow, Modeling, Computers, Ripple, Cracking, Grain, Size.

20. ABSTRACT (Continue on reverse side if necessary and identify by block number)

Pulsed current gas tungsten arc welds made in Fe-26Ni alloy and AISI 321 stainless steel were dimensionally and structurally analyzed. Weld pool kinetics, weld surface ripple formation and weld solidification structure were studied using high speed motion pictures, conventional and scanning electron metallography, and x-ray dispersive analysis. Varestraint tests were performed on AISI 321 and 316 stainless steel sheets to study the effects of grain refinement on the properties of the weld metal and its hot cracking tendency. (cont.)

DD FORM 1 JAN 73 1473 EDITION OF 1 NOV 65 IS OBSOLETE

376635

SECURITY CLASSIFICATION OF THIS PAGE (When Data Entered)

20. ABSTRACT (cont.)

A two-dimensional heat flow computer model, utilizing an explicit finite difference technique, was developed to predict temperature fields, thermal gradients, the solidus and the liquidus movement and weld pool size and shape at anytime during the course of the welding operation. Results indicate pulsed arc welding process can be manipulated to influence mixing in the weld pool, grain morphology and size in the solidified weld metal and its properties, i.e., hot cracking tendency. Computer simulations of the heat flow can provide accurate predictions of the thermal regime occurring at and around the weld pool during welding.

TABLE OF CONTENTS

R&D Report 81-9D4-PULSE-R1 March 4, 1981

INVESTIGATION OF WELD POOL STRUCTURE AND PROPERTY CONTROL IN PULSED ARC WELDING

G. M. Ecer and G. G. Lessmann
Westinghouse R&D Center
Pittsburgh, PA 15235

and

H. D. Brody
University of Pittsburgh
Pittsburgh, PA

ABSTRACT

Pulsed current gas tungsten arc welds made in Fe-26Ni alloy and AISI 321 stainless steel were dimensionally and structurally analyzed. Weld pool kinetics, weld surface ripple formation and weld solidification structure were studied using high speed motion pictures, conventional and scanning electron metallography, and x-ray dispersive analysis. Varestraint tests were performed on AISI 321 and 316 stainless steel sheets to study the effects of grain refinement on the properties of the weld metal and its hot cracking tendency. A two-dimensional heat flow computer model, utilizing an explicit finite difference technique, was developed to predict temperature fields, thermal gradients, the solidus and the liquidus movement and weld pool size and shape at any time during the course of the welding operation. Results indicate pulsed arc welding process can be manipulated to influence mixing in the weld pool, grain morphology and size in the solidified weld metal and its properties, i.e., hot cracking tendency. Computer simulations of the heat flow can provide accurate predictions of the thermal regime occurring at and around the weld pool during welding.

FORWARD

This final report was prepared by the Westinghouse Electric Corporation in collaboration with the University of Pittsburgh, under Office of Naval Research Contract N00014-77-C0596, "Investigation of Weld Pool Structure and Property Control in Pulsed Arc Welding". The program was administered under the technical direction of the Office of Naval Research, Department of the Navy, Arlington, VA, with Dr. Bruce A. MacDonald (Code 471) serving as the ONR Scientific Officer in charge of inspection and acceptance of the program.

The project work was carried out by the Westinghouse Electric Corporation with the University of Pittsburgh, Metallurgical and Materials Engineering Department acting as a subcontractor.

The Westinghouse part of the program was managed by Mr. G. G. Lessmann, Manager of Metals Joining and Metals Processing, and technically directed by Dr. G. M. Ecer. Significant contributions were also made by T. Mullen (x-ray dispersive analysis), R. Berrier (metallography, welding set-up, Varestraint testing), W. R. Kuba (welding set-up), R. Kuznicki (x-ray diffraction), A. J. Heim and J. Rogy (hot and cold rolling), D. F. Baker (vacuum melting), J. Yex (metallography) and K. A. Grande (typing). In addition, M. M. Downs was involved in the preparation of the computer software.

The University of Pittsburgh part of the program was managed and technically directed by Dr. H. D. Brody, Professor of Metallurgical and Materials Engineering. Mr. M. Vassilaros prepared the initial computer model as part of a course project. Mr. Tri Dinh contributed to modifications of the program and performed the correlations with experiment. Mr. A. Gokhale was initially involved in cinematographic analysis of weld pool kinetics, later conducted a study on hot cracking and weld zone structural control in AISI 316 and AISI 321 stainless steels as part of his M.S. thesis. Prof. Alexander Tzavaras of Aristotelian University, Salonika, Greece, participated in the project from June through October 1978 as a visiting professor. Ms. L. Smith, Mr. J. Farinelly, Ms. M. A. Krenicky and Mr. J. Gasper have helped in metallographic specimen preparation. Mr. G. M. McManus and Dr. R. Sinha aided with SEM analysis.

TECHNICAL BACKGROUND

The area of weld metal solidification related to pulsed-current welding has more parametric freedom than conventional steady-current methods, mainly because of the additional process parameters that are brought about by current pulsation. Intelligent control of these parameters (that is, high and low currents and their respective times) may allow the resultant thermal and arc pressure fluctuations to be used as vehicles of structural control. Variations in the arc force acting on the weld, for example, may increase turbulence in the weld puddle, resulting in the dendrite fragmentation that promotes nucleation of many grains of smaller size than those developed under steady current welding. Periodic and extensive temperature fluctuations in the weld zone may influence solute build-up along the weld seam.

Fine grain size is generally preferred in weldments for two reasons: (1) it gives improved properties, and (2) it decreases solidification crack susceptibility.[1] Although potent grain refiners (inoculants) could be added to refine the grain size, this technique is not widely practiced because of the complexity of chemical side effects of inoculants. Pulsing, on the other hand, has potential for systematic and reliable control of fusion zone grain size, irrespective of the metallurgical system.[2]

Pulsed-current welding is a relatively new technology. It has been applied to a variety of welding processes: gas tungsten arc (GTA), gas metal arc, shielded metal arc, electron beam, plasma arc, submerged arc, and laser. Literature on the subject has already grown to an impressive size: over 250 articles have appeared, mainly in Russian journals, within the last 15 years. Much of the interest in pulsed current welding has centered on its application to GTA welding. This is reflected both in the number of technical articles published on the subject, and in the number of pulsed-current gas tungsten arc welding power supplies sold in the United States. Over 45 percent of all GTA power sources sold within the last three years by Hobart Brothers, for example, had built-in pulsing capability.[3]

Pulsed current, in GTA welding, produces a continuously welded seam consisting of overlapping arc spot welds. In its simplest form, welding current is switched between a high level that produces the arc-spot weld and a low level that only serves to maintain the arc. Because the weld pool is allowed to cool between pulses and the heat is dissipated in the work, the effects of heat buildup or disparity in heat sink are largely overcome.[4] Some investigators,[5-7] therefore, report much better penetration control with pulsed-current GTA than with steady-current GTA. The slag buildup problem that is common in welding certain steels (such as maraging steels) is also eliminated,[4] for the same reason. Other benefits attributed to pulsing include residual stresses,[8,9] structural refinement,[10-12] higher resistance to hot cracking,[11-13] reduced width of the heat-affected zone,[5] and improved mechanical properties.[8,10,11]

Structural refinement, higher resistance to hot cracking, and the improved mechanical properties reported in the literature are most often achieved by selecting the pulsed welding variables so as to produce a favorable range of cooling rates along the weld seam, as well as to influence the primary and secondary solidification patterns of the weld pool. In turn, the mode of solidification largely governs the weld metal properties by influencing the grain size and orientation, the phases precipitated, and the segregation processes that affect hot cracking.

INTRODUCTION

In the initial proposal to the Office of Naval Research, the Westinghouse Electric Corporation proposed an investigation of weld pool structure and property control in pulsed arc welding in which solidification theories would be applied to the interpretation of weld metal structures developed under pulsed arc welding. The purpose was to control weldment properties by establishing relationships between the properties and the weld process variables. Work began in 1978 under Contract N00014-77-C-0596; the University of Pittsburgh participated as a subcontractor to Westinghouse. The overall objectives of the project were: (1) to develop a predictive model relating welding process variables to weld solidification structure, and (2) to demonstrate the feasibility of controlling weld properties by use of this model. These objectives were largely met at the end of the three year study, the major results of which are presented here.

Briefly, the first year's effort focused on the development of a predictive mathematical model of pulsed arc welding of thin sheets (two dimensional heat flow), and on the establishment of experimental techniques. In the second year, the model was refined to accommodate more realistic welding conditions, and a predictive model was developed for the welding of thick plates (three-dimensional heat flow). But, due to restrictions in time and increased interest in other parts of the study, the 3-D model was not evaluated. Later in 1979, work was initiated on the effects of pulsed arc welding on segregation processes; this effort focused on the problem of hot cracking as affected by pulsation of the heat input. High speed cinematographic observations of the weld pool were incorporated into the Fiscal Yeat-79 and Fiscal Year-80 programs as a means of studying the weld pool kinetics under pulsing.

Work in Fiscal Year-80 concentrated on testing of the two-dimensional heat flow model against experimental measurements while incorporating further improvements into the model. Effect of pulsed

current waveform on hot cracking tendency and the weld solidification structures formed in Types 316 and 321 stainless steels were studied.

This final report is presented in three parts in the form they are submitted for publication:

Part I - Weld Pool Fluid Motion and Ripple Formation in Pulsed-Current GTAW

Part II - Heat-Flow Simulation of Pulsed Current Gas Tungsten Arc Welding

Part III - Grain Structure and Hot Cracking in Pulsed Current GTAW of AISI 321 Stainless Steel

A complete list of the publications on the results obtained in this study is given below.

LIST OF PUBLICATIONS

1. A. Tzavaras, M. Vassilaros, H. Brody, and G. Ecer, "Effect of Welding Parameters on Solidification Structures in Pulsed GTA Welded Fe-26Ni", in Physical Metallurgy of Metal Joining (Eds. R. Kossowsky and M. E. Glicksman), Conf. Proceedings, TMS-AIME, Warrendale, PA (1980).

2. H. D. Brody and R. A. Stoehr, "Computer Simulation of Heat Flow in Casting", Journal of Metals, 32 (9), 20-27 (Sept. 1980).

3. G. M. Ecer, A. Tzavaras, A. Gokhale and H. D. Brody, "Weld Pool Fluid Motion and Ripple Formation in Pulsed-Current GTAW", TMS-AIME Fall Meeting, Pittsburgh, PA (Oct. 1980). Submitted for publication in the Welding Journal.

4. G. M. Ecer, M. Downs, H. D. Brody and A. Gokhale, "Heat-Flow Simulation of Pulsed Current Gas Tungsten Arc Welding", to be published in Proc. Conf. on Modeling of Casting and Welding Processes, sponsored by Engineering Foundation, ASM and AIME, Rindge, NH (Aug. 3-8, 1980).

5. A. A. Gokhale, H. D. Brody, and G. M. Ecer, "Grain Structure and Hot Cracking in Pulsed Current GTAW of AISI 321 Stainless Steel", presented at ASM Materials and Processes Congress, Cleveland, OH (Oct. 30, 1980). To be submitted for publication in the Welding Journal.

6. A. A. Gokhale, "Weld Pool Solidification Structure and Property Control in Pulsed Current Gas Tungsten Arc Welding", M.S. Thesis, University of Pittsburgh, Advisor: H. D. Brody (1980).

CONCLUSIONS

1. In simulating the heat flow in pulsed arc welding, the explicit finite difference technique has been found adequate in predicting temperature fields, thermal gradients, the solidus and the liquidus movement as well as weld pool size and shape at anytime during the course of the welding operation.

2. The simplifying assumptions made by selecting constant values for the relevant material thermal properties did not seem to have had a major impact on the accuracy of the computed results as determined by comparisons with experimental findings.

3. Three types of weld fluid motion are observed in thin sheet PC-GTAW. These are:

   (a) Radially moving flow initiated by the changes in arc pressure;

   (b) Rotational flow presumably electromagnetic in origin and located near the anode spot region;

   (c) Up and down oscillating motion, again, triggered by the sudden changes in arc pressure.

   Radial flow is a more effective vehicle of mixing in the weld pool, but is short lived. Higher pulsing frequencies for a given heat input should, therefore, result in more complete mixing in the pool.

4. The up and down oscillations of the fluid in the weld pool have a constant period. These oscillations cyclicly provide liquid metal reservoirs above the weld surface into which solid can grow. Such growth constitutes a ripple made up of tiny spikes protruding from the workpiece surface and delineates the solidus isotherm existing at the time of their formation. Ripple spacings may be used to estimate local solidification rates in pulsed current GTA welds.

5. Grain structure in the weld bead can be refined by adjusting the pulsing parameters. Low t_p/t_b ratio (0.1-0.2), high pitch (2-3 mm), and arc modulation seem to be beneficial in grain refining weld bead microstructure.

6. Weld bead microstructure influences hot cracking susceptibility in AISI 321 stainless steel. The occurrence of hot cracking is reduced by having a predominantly equiaxed structure and having a fine grain size.

REFERENCES

1. J. G. Garland, "Weld Pool Solidification Control", Metal Constr. and Br. Welding J., 121-128 (April 1974).

2. G. J. Davies and J. G. Garland, "Solidification Structure and Properties of Fusion Welds", International Met. Reviews, 20:83-106 (1975).

3. Personal communication with Ralph Barhorst, Hobart Bros. Technical Center, Troy, Ohio (April 13, 1977).

4. J. C. Needham, "Pulsed Current Tungsten Arc Welding", paper in Pulsed TIG Welding Seminar Handbook, Brit. Weld. Inst., Abington, Cambridge (1973).

5. P. Boughton, "High Precision Pulsed TIG-Welding", paper in Pulsed TIG Welding Seminar Handbook, Brit. Weld. Inst., Abington, Cambridge (1973).

6. P. Boughton and B. O. Males, "Penetration Characteristics of Pulsed TIG-Welding", paper in Pulsed TIG Welding Seminar Handbook, Brit. Weld. Inst., Abington, Cambridge (1973).

7. G. G. Cherng and V. A. Danilov, "Calculating Pulsed-Arc Welding Conditions", Auto. Weld., 26 (9): 11-14 (1973).

8. L. M. Lobanov, A. S. Karpenko, L. M. Chertov, and I. M. Zhdanov, "Special Features of the Technology for the Pulsed Arc Welding of D-20 Alloy, and Determination of the Residual Stresses in Joints", Auto. Weld., 28 (2):12-15 (1975).

9. R. G. Dickens and B. E. Pinfold, "Investigations in Pulsed Tungsten Inert-Gas Welding", paper in Pulsed Tig Welding Seminar Handbook, Birt. Weld. Inst. (1973).

10. G. A. Slavin, et.al., "Control of the solidification Process by Means of a Dynamic Action of the Arc", Weld. Prod., 21 (8):2-3 (1974).

11. U. I. Birman and A. V. Petrov, "Influence of the Weld Metal Solidification Pattern on Hot Cracking During Pulsed-Arc Tungsten-Electrode Welding", Weld. Prod., 18 (6):22-25 (1971).

12. A. V. Petrov and V. I. Birman, "Solidification of Weld Metal in Pulsed Arc Welding", Weld. Prod., 15 (6):1-5 (1968).

13. G. A. Slavin, et.al., "The Structure and Solidification Cracking Resistance of Aluminum Alloy D20 in Pulsed Arc Welding", Weld. Prod., 21 (6):34-37 (1974).

PART I

WELD POOL FLUID MOTION AND RIPPLE FORMATION IN PULSED-CURRENT GTAW

G. M. Ecer
Westinghouse R&D Center
Pittsburgh, PA 15235

A. Tzavaras
Aristotelian University
Salonika, Greece

A. Gokhale and H. D. Brody
University of Pittsburgh
Pittsburgh, PA

ABSTRACT

High speed motion picture observations of pulsed current-GTA weld pools produced in thin sheets of Fe-26Ni alloy show three types of fluid motion. A radially moving flow, dominant in the early high and low pulse times, is initiated by the sudden changes in the arc pressure. The larger the change in current or its rate of change, the faster is the flow. A second fluid motion, electro-magnetic in origin, exists near the anode spot region and consists of two symmetrical rotational flows. Thirdly, an up and down oscillation motion is triggered by the changes in arc pressure.

The up and down oscillations have a constant period which provide markers, indicative of the solidus isotherm, on the weld surface by forming ripples. Each ripple is composed of tiny spikes that protrude from the weld surface. They form at times when pool oscillations provide reservoirs of liquid above the plane of solid at the solidus isotherm. Because the time intervals between ripple formation are constant, ripple spacings are indicative of the local solidification rates.

INTRODUCTION

Weld pool fluid motion is known to influence weld bead shape[1-5], heat transfer within the weldment[5,6], chemical homogeneity of the weld metal[7-10], extent of gas-metal-slag reactions[9,10], defect formation[11,12] and solidification structure[13,14]. These effects, often interdependent, more or less characterize properties of a weld, yet, the all important common denominator, namely the fluid motion, has been studied very little. In steady-current arc welding, in the absence of arc oscillations and mechanical or magnetic forces applied for stirring, the motion in the pool has been attributed, with some controversy, to Lorentz's force[3,9], mechanical force effect of the arc[15,16] and to the differences in the surface tension of various parts of the weld pool[11]. In pulsed-current arc welding, on the other hand, there seems to be no observations on weld pool motion reported in the open literature.

In pulsed-current gas tungsten arc welding (PC-GTAW), cycling of the arc current between a high pulse current (i_p) and a low pulse current (i_b) (Figure 1) results in cyclic changes in heat input, arc pressure on the weld pool, radial temperature and pressure distribution and weld pool shape. In addition, fluid motion in the pool is affected by the pulsating arc. The present study reports some observations on the fluid motion in the weld pool formed under a pulsed-current gas-tungsten arc, and provides an explanation for the formation of weld surface ripples, as well as suggesting ways of utilizing ripple spacing for estimation of local solidification rates.

The subject of weld surface ripples has been considered previously and a number of theories have been suggested to explain their formation. For example, D'Anessa[17] proposed that interaction of growth rate fluctuations and surface tension effects was responsible for the ripples. Garland[18], on the other hand, concluded that the ripples could not be due to growth rate fluctuations, but were related to the cyclic current supply. He, then, suggested a mechanism involving

an interface/liquid surface interaction at rapid rates of solidification. An earlier work by Cheever and Howden[19] attributed ripples to the existence of growth rate fluctuations caused by the solid-liquid interface instability presumed to be inherent to rapid solidification. Later, Kotecki, Cheever and Howden[20] showed that pool oscillations caused by the physical pressure of an arc plasma produced the ripples. It is with this final proposal that our observations seem to agree.

EXPERIMENTAL

Observations on weld pool fluid motion were made by preparing high speed motion pictures of a number of PC-GTA welds. Figure 2 is a schematic of the clamping fixture used to make full penetration welds in 0.08 cm thick sheets of the Fe-26Ni alloy. The tungsten arc moved normal to the plane of the sketch in the direction of the ground connection. The arc length was kept constant at 0.1 in. (0.25 cm). The use of Teflon, with a thermal conductivity of about 250 times less than that of the Fe-26Ni alloy, was to minimize the influence of the grips on removal from the weld zone. The latter condition was imposed mainly to satisfy the assumptions made in the development[21] of a two-dimensional heat flow model of the pulsed-current arc welding.

In addition to the above, the following parameters were kept constant: electrode composition, size and shape were W + 2% ThO_2, 1/8 in. (0.32 cm) diameter, 30° included vertex angle with 0.04 in. (0.1 cm) diameter flat tip; 100% argon as shield gas flowing at a rate of 40 cfh (18.9 ℓ/min) from around the electrode and 4 cfh (1.9 ℓ/min) to the back of the weldment; electrode stick-out from the cup 0.5 in. (1.25 cm) and from the collet 1.16 in. (2.95 cm). All welding was done with direct current electrode negative. Pulsed current waveform remained nearly square shaped within the pulse frequency range of 1 to 100 Hz.

High speed motion picture observations of weld pool from the trailing edge direction (Figure 3) and from the side were made when the weld puddle reached a steady size. The camera speed increased to about 1000 frames/sec. after the first 0.3 seconds of operation. A pulsating red light within the camera provided markers on the film at a rate of 100 markers per second for more precise measurements of the camera speed. The films produced were analyzed using a professional editing machine with the capacity to record lapsed time and frame sequence electronically. Both frame by frame analysis and viewing at various speeds were made.

RESULTS AND DISCUSSION

Weld Pool Fluid Motion in High Pulse Time, t_p

High speed motion pictures of the weld pool indicate three types of fluid motion in the PC-GTA weld pool. When the steady state pool size is reached, these motions in the pool become repetitive from one pulse cycle to the next, but differ within the high pulse and low pulse times.

Initially in the high pulse time (t_p), with the onset of the high pulse arc ($i_b \rightarrow i_p$), the sudden increase in the arc pressure causes an outward rush of the liquid metal from under the arc. The wave thus formed moves "radially" to the solid-liquid interface and is partially reflected from there, initiating a wave radially moving inward. This radial back and forth motion dampens quickly giving way to a "rotational" motion, or makes the already existing rotational motion more predominant. After the initial radial wave reaches the solid-liquid interface, and some of the liquid is reflected inward, there still remains an excess pressure within the liquid metal causing the pool surfaces to slightly bulge out, as depicted in Figure 4(a), all during t_p. The sudden increase in the fluid pressure at a given point in the pool is opposed by the surface tension of the pool at top and bottom surfaces. Until the two opposing pressures become equal, an up and down "oscillating" motion is triggered by the increase in arc pressure with $i_b \rightarrow i_p$ transition.

These three motions, simply referred to as radial, rotational and oscillating, are shown as arrows A, B and C in the schematic representations in Figure 4.

The speed of the radial flow (A) during t_p was measured as high as 450 mm/sec in the direction of the trailing edge of the pool for i_p = 150 amps. For a high pulse current of i_p = 120 amps the maximum radial flow speed was just less than 200 mm/sec., indicating the strong

influence of the arc current on the mixing in the pool. The maximum surface fluid flow, measured by following oxide particles on the pool surface, in all cases occurred within the first 10 milliseconds after the high pulse current was on. Radial flow speed typically slowed down quickly to negligible values, as seen in Figure 5, and later reversed direction. For high pulse times much longer than about 100 ms, the radial flow (A) contributes little or nothing to pool mixing. Only the rotational fluid flow remains all throughout t_p, leaving a large segment of the trailing portion of the weld pool relatively motionless. For the same heat input, radial flow speed (v_A) is higher for smaller t_p values. For example, when i_p = 150 amps, i_b = 10 amps and t_p/t_b = 0.62, the maximum value of v_A can be about 430 mm/sec. for t_p = 0.020 sec., but it only reaches 180 mm/sec. if t_p = 0.208 sec. Presumably because for larger t_b values high pulse arc pressure is exerted on a cooler weld pool which is expected to have higher surface tension and lower fluidity.

In the present study, weld pool fluid flow observations were conducted for pulsed current welds having i_p values of 120 and 150 amps and i_b of 10 amps in all cases. Under these restricted conditions, the rotational fluid motion (B in Figure 4) became apparent after about 10 to 20 ms into t_p, and became predominent after about 40 ms of t_p had elapsed. This effect was mainly a result of the radial flow's lessening speed, rather than the increasing severity of the rotational flow. The maximum v_B increased with higher i_p, i.e., from a value of 140 mm/sec. to 330 mm/sec. for i_p values of 120 amps and 150 amps respectively. For t_p values up to 0.208 sec. the rotational flow was observable with little loss in its speed.

The up and down oscillation motion of the liquid during t_p was readily observable at the trailing edge from reflections of the hot tungsten electrode in the pool. It quickly dampened so that no more than three or four periods of the motion could be counted. The arc pressure on the weld pool was felt at the trailing edge of the pool (8 mm away from the center of the anode spot) within the first 9-11 ms of t_p.

Weld Pool Fluid Motion in Background Pulse Time, t_b

The arc plasma pressure on the pool is released when $i_p \rightarrow i_b$ transition occurs. The liquid metal pushed against the solid-liquid interface by the high pulse arc pressure, when released leads to a flow that moves radially inward (A in Figure 4(b)). This radial flow, changing direction several times, slows down and gives way to a relatively calm weld pool, as typically represented by the plots in Figure 6.

During t_b, when the welding arc was maintained by only a 10 amps low pulse current in the present study, rotational fluid flow (B in Figure 4(b)) was barely detectable. Its speed was generally less than 25 mm/sec.

The rotational motion, both during t_p and t_b, was always confined to the forward and central portion of the pool, covering only about 1/2 of the total pool surface. Its speed was generally slightly higher in the forward section than in the central section of the pool.

The oscillating up and down motion during t_b could be seen more clearly than that occurring during t_p. Through observations of the reflection of the hot electrode tip on the oscillating weld pool (Figure 7) it was possible to determine the period of oscillation for several pulsed current welds as seen in Table 1. These observations were made while the camera was located at the weld centerline and focused at the trailing portion of the weld pool, just as sketched in Figure 3. It is seen that after the first two reflections, the time intervals between reflections appearing at the weld pool trailing edge became constant. The period of these oscillations remained almost identical for a given set of pulsed current welding parameters in different welds, as well as in different low pulse periods within the same weld.

Timing of the first two reflections were seemingly unrelated to those of the subsequent reflections, although they too were quite reproducible. The difference could be due to the interference of the radial flow which decays quickly within the first 30-50 milliseconds after $i_p \rightarrow i_b$ transition.

Arc Pressure Considerations

The radial fluid flow, unlike the rotational flow, can sweep along the trailing edge of the pool, thus it has a more pronounced effect on solidification processes than the rotational flow. The degree of mixing due to this radial motion probably depends on the amplitude and the rate of change in arc current since arc pressure is related to the arc current. An expression developed by Maecker has been the basis of analysis[22] of the gas pressure of a cylindrical electric arc. For welding arcs, if Maecker's expression is assumed to apply, an expression could be written relating gas pressure of the arc, P(r), at a distance r away from the arc axis, to the arc current, i, and the anode spot radius, r_a:

$$P(r) = k \frac{i^2}{r_a^2} \left(1 - \frac{r^2}{r_a^2}\right)$$

where k is a constant. In pulsed current arc welding i and r_a change cyclicly as dictated by the arc current waveform. Early in the high pulse period the rate of increase of the arc current is much higher[23] than that of the size of the anode spot leading to a higher (up to 50%) initial arc pressure. While dr_a/dt is largely dependent on the weld metal chemistry[24], di/dt is fixed by the type of power source used.

The transistorized power supply (Astro-Arc Model CA-150-TS) used in the present investigation produced nearly square waveforms between frequencies 0.5 and 100 Hz, and up to i_p = 150 amps. At the highest frequencies, waveform square shape was slightly lost (Figure 8) leading to a time lag of about 1.5 milliseconds before a current rise from 30 to 120 amps could take place. Much of this rise occurred within the first 0.2 milliseconds of t_p, (di/dt was about 380 k.amps/sec.). In comparison, the size of the anode spot is expected to continually increase for comparatively longer times. For example, Ludwig's[24] data on stainless steels showed that anode spot size peaked at around 10 seconds. The effect of the arc pressure could presumably be

accentuated by increasing the portion of t_p in which higher arc pressures are expected and experienced[23]. This could simply be done by increasing pulse frequency for the same t_p/t_b ratio.

It is reasonable to suggest, therefore, that in pulsed-current arc welds, for a given heat input, more mixing in the weld pool will occur when the pulsing frequency is reduced. This mixing would largely be a result of the increased predominance of the radial flow.

Lorentz Force and Surface Tension Effects

While the observations on the radial flow indicate it to be caused by the gas-pressure component of the welding arc, the longer lasting but slower rotational flow is more likely a result of the current-magnetic field interaction.

The double circulating pattern of the rotational flow observed in this study was similar to the pattern obtained by Woods and Milner[9] in simulations of weld pools with pools of mercury in the absence of an arc plasma jet action. Furthermore, the persistence of the rotational flow long after the radial flow had dampened out points to the rotation being induced by crossed magnetic and electric fields. Forces created by such interaction cause an excess pressure region, in the liquid beneath the arc, which is equal and opposite to the Lorentz force. The excess pressure leads to the stirring of the liquid whose velocity is proportional to the product of the current and the field strength[9].

The surface tension of the liquid-gas interface is the only force opposing the combined actions of the gravity and arc gas-pressure in thin sheet full penetration welds where the weld pools form under nearly two-dimensional heat removal conditions. When the arc pressure increases or decreases in parallel with current cycling, arc depression accordingly

increases or shrinks toward an equilibrium size dictated by the force balance between surface tension, gravity and arc pressure. It is easy to see, therefore, that when the surface tension is high, arc depression will be low and so will the radial flow strength. The up and down harmonic motion too is dependent on surface tension in that the oscillation amplitude and its period[20] will be influenced by it.

Mechanism of Weld Surface Ripple Formation

After reviewing the high-speed motion pictures of eleven welds made on thin sheets of the Fe-26Ni alloy, the following main features of the mechanism of formation of weld surface ripples in pulsed current welding have emerged.

The oscillating motion of the liquid at the growing solid-liquid interface provides a temporary reservoir of liquid metal, above the surface plane of the sheet metal, into which solid growth can take place. At the back of the weld the temporary reservoir of liquid is below the sheet surface. Solid growth normal to the plane of the workpiece occurs all along the solidification isotherm constituting a ripple on the solidified weld metal (Figure 9). At higher magnifications, as typically shown in Figure 10, ripples are seen as made up of individual spikes which tend to form at solidification cell boundaries, as in Figure 11. Figures 9-11 are views of a PC-GTA weld made in the Fe-26Ni alloy with the following weld parameters: i_p = 140 amps; i_b = 10 amps; t_p = 0.167 sec.; t_b = 0.667 sec.; and arc travel = 0.212 cm/sec.

Since the ripples form when weld pool oscillations periodically provide molten metal above or below the planes of the weld top or bottom surfaces, as suggested above, they should then reflect the chemistry of the solute rich boundary layer just ahead of the solid-liquid interface. This was clearly the case when spikes and nearby spike-free areas of the weld metal surface were analyzed by the energy dispersive x-ray method. Approximately calculated percentages of silicon and manganese, minor elements in the bulk alloy, were considerably higher in the spikes

than found in the nearby flat areas. Table 2 gives the compositional ratios of five elements found in the spikes. Aluminum found in the alloy was an unintentional impurity.

Solidification Rates From Ripples

Aside from acting like markers showing the shape of solidification isotherms along the weld seam, weld surface ripples may contain other information that could be useful in analysis of weld pool phenomena and in weld quality assurance. An example is ripple spacing. Under precisely controlled welding conditions, such as those that could exist in mechanized welding, the repetitive nature of the ripples could provide clues to any momentary fluctuation in the weld solidification rate or to the formation of weld defects.

In analysis of weld solidification under pulsed welding conditions, one of the determinants is the solidification rate. Although the average rate is equal to the arc travel speed, the pulsed nature of the heat input dictates periodic increases and decreases in the rate of solidification. Approximate measurements of such variation may be possible from the ripple spacings.

Experimentally determined times for successive reflections of the electrode appearing at the trailing edge of the pool are tabulated in Table 1. It is seen that after the second or third reflection, a relatively constant pool oscillation period is reached, yet the secondary ripple spacings, as seen in Figure 10, change with distance along the weld axis. The unequal ripple spacings result from the variations in the solidification rate between pulses. It should, therefore, be possible to determine local rates of solidification from ripple spacings.

In Figure 12 a comparison is made between the measurements of solid-liquid interface displacement after $i_p \rightarrow i_b$ transition for a PC-GTA weld. Only the displacement of the trailing edge of the weld pool is measured. Measurements obtained from ripple spacings of two

separate welds are very close. Agreements with the displacement measurements from a high speed motion picture and computed curves are also good. An explicit finite difference technique was used to obtain the computed solidus and liquidus movements shown in the figure. The computational model simulated heat flow for PC-GTAW for two dimensional conduction and have been described elsewhere[25,26]. In the present work, the computational model was more sensitive than the motion picture observations of the solidus and liquidus. In the motion pictures due to the diffused nature of the light radiation from the mushy zone of the pool it was very difficult to distinguish between the locations of the solidus and liquidus, so that an intermediate boundary between them was followed for the measurements shown in Figure 12. It is noteworthy that the growth distances calculated from ripple spacings are closer to the solidus curve than to the liquidus as would be expected from the mechanism of ripple formation described above.

Additional information that can be obtained from ripples is the average growth and growth rates for high pulse and low pulse periods. The transitions from i_p to i_b and vice versa create waves that have high amplitudes initially. The first ripples that form after each transition, therefore, are markedly more visible than the others. Measurements of the distance between these high intensity ripples then give the total solid-liquid interface displacements during t_p or t_b. Distances solidified, S_p and S_b, in these two periods and the average rates of solidification, R_p and R_b, may be determined easily. These quantities may then be used to assess the effect of a given pulsing parameter on changes in solidification rates within a pulse period. Figure 13 shows pulse frequency effect for a series of welds made under two dimensional heat flow conditions and a constant heat input. [Heat input in PC-GTAW for nearly square current waveforms can be calculated from

$$H = \frac{1}{4.184\theta} (e_p i_p t_p + e_b i_b t_b) \text{ cal/cm}$$

where 4.184 comes from converting joules to calories, and e is the arc voltage for corresponding arc current.]

CONCLUSIONS

1. Three types of weld fluid motion are observed in thin sheet PC-GTAW. These are:

   (a) Radially moving flow initiated by the changes in arc pressure;

   (b) Rotational flow presumably electromagnetic in origin and located near the anode spot region;

   (c) Up and down oscillating motion, again, triggered by the sudden changes in arc pressure.

2. Radial flow is a more effective vehicle of mixing in the weld pool, but is short lived. Higher pulsing frequencies for a given heat input should, therefore, result in more complete mixing in the pool.

3. The up and down oscillations of the fluid in the weld pool have a constant period. These oscillations cyclicly provide liquid metal reservoirs above the weld surface into which solid can grow. Such growth constitutes a ripple made up of tiny spikes protruding from the workpiece surface and delineates the solidus isotherm existing at the time of their formation.

4. Ripple spacings may be used to estimate local solidification rates in pulsed current GTA welds.

ACKNOWLEDGEMENT

Funding by the Office of Naval Research Contract is gratefully acknowledged.

REFERENCES

1. Mills, G. S., "Weld Pool Motion in GTA Welding: Importance and Description", Proceedings of the Fifth Bolton Landing Conference on Weldments: Physical Metallurgy and Failure Phenomena, August 1978 (General Electric Co., Schenectady, NY) pp. 329-337.

2. Glickstein, S. S., "Arc-Weld Pool Interactions", Ibid, pp. 339-351.

3. Bukarov, V. A., Ishchenko, Yu. S., and Loshakova, V. G., "The Effect of the Convection of Metal in the Weld Pool on Penetration", Welding Production, 25 (11) 1978, pp. 5-9.

4. Friedman, E., "Analysis of Weld Puddle Distortion and its Effect on Penetration", Welding Journal, 57 (6), 1978, Research Suppl., pp. 161-s to 166-s.

5. Christensen, N., Davies, V. de L., and Gjermundsen, K., "Distribution of Temperatures in Arc Welding", British Welding Journal, 12 (2) 1965, pp. 54-75.

6. Apps, R. L. and Milner, D. R., "A Note on the Behaviour of Liquid Metal Under the Arc", British Welding Journal, 10 (7) 1963, pp. 348-350.

7. Houldcroft, P. T., "Dilution and Uniformity in Aluminum Alloy Weld Beads", British Welding Journal, Vol. 1, 1954, p. 468.

8. Pumphrey, W. I., "Weld Metal Dilution Effects in the Metal Arc Welding of Al-Mg-Si Alloys", British Welding Journal, 2 (1) 1955, p. 93.

9. Woods, R. A. and Milner, D. R., "Motion in the Weld Pool in Arc Welding", Welding Journal, 50 (4) 1971, Res. Suppl., pp. 163-s to 173-s.

10. Salter, G. R., and Milner, D. R., "Gas-Metal Reactions in Arc Welding", British Welding Journal, 12 (5) 1965, pp. 222-228.

11. Bradstreet, B. J., "Effect of Surface Tension and Metal Flow on Weld Bead Formation", Welding Journal, 47 (7) 1968, Res. Suppl., pp. 314-s to 322-s.

12. Savage, W. F., Nippes, E. F., and Agusa, K., "Effect of Arc Force on Defect Formation in GTA Welding", Welding Journal, 58 (7) 1979, Res. Suppl., pp. 212-s to 224-s.

13. Davies, G. J. and Garland, J. G., "Solidification Structures and Properties of Fusion Welds", International Metallurgical Reviews, 20 (196) 1975, pp. 83-106.

14. Tadashi, M., and Ikawa, K., "The Relationship Between the Convective Flow Rate Controlled by Lorentz's Force and the Solidified Structures", Trans. Jap. Institute of Metals, Vol. 19, 1978, pp. 537-545.

15. Kovalev, I. M., "Investigation of Currents of Liquid Metal in Argon-Arc Welding with a Non-Consumable Electrode", Welding Production, 21 (9) 1974, pp. 16-19.

16. Bukarov, V. A., et.al., "On the Force Effect of a Constricted Arc on the Welded Metal", Welding Production, 23 (6) 1976, pp. 4-6.

17. D'annessa, A. T., "Sources and Effects of Growth Rate Fluctuations During Weld Metal Solidification", Welding Journal, 49 (2) 1970, Res. Suppl., pp. 41-s to 45-s.

18. Garland, J. G., and Davies, G. J., "Surface Rippling and Growth Perturbations During Weld Pool Solidification", Metal Constr. and British Welding Journal, 2 (5) 1970, pp. 171-175.

19. Cheever, D. L. and Howden, D. G., "Technical Note: Nature of Weld Surface Ripples", Welding Journal, 48 (4) 1969, Res. Suppl. pp. 179-s to 180-s.

20. Kotecki, D. J., Cheever, D. L., and Howden, D. G., "Mechanism of Ripple Formation During Weld Solidification", Welding Journal, 51 (8) 1972, Res. Suppl., pp. 386-s to 391-s.

21. Tzavaras, A., Vassilaros, M., Brody, H., and Ecer, G., "Effect of Welding Parameters on Solidification Structures in Pulsed GTA Welded Fe-26%Ni", in Physical Metallurgy of Metal Joining (Ed's: R. Kossowsky and M. E. Glicksman), The Metallurgical Society of AIME, Warrendale, PA, 1980, pp. 82-116.

22. Maecker, H., Z. Physik, Vol. 141, 1955, p. 198, as cited by Milner, D. R., et.al., in "Arc Characteristics and Their Significance in Welding", British Welding Journal, 7 (2) 1960, pp. 73-88.

23. Barabokhin, N.S., et.al., "The Gas-Dynamic Pressure of an Open Pulsed Arc", Welding Production, 23 (2) 1976, pp. 5-8.

24. Ludwig, H. C., "Current Density and Anode Spot Size in the Gas Tungsten Arc", Welding Journal, 47 (5) Res. Suppl. (1968).

25. Brody, H. D. and Stoehr, R. A., "Computer Simulation of Heat Flow in Casting", Journal of Metals, 32 (9) 1980, pp. 20-27.

26. Ecer, G. M., Downs, M., Brody, H. D., and Gokhale, A., "Heat Flow Simulation in Pulsed-GTA Welding", Proc. of Engineering Foundation Conf. on Modeling of Casting and Welding Processes, August 3-8, 1980, Rindge, NH.

TABLE 1

TIMES OF THE TUNGSTEN ELECTRODE REFLECTIONS SEEN AT
THE TRAILING EDGE OF THE WELD POOL DURING A LOW PULSE TIME
The Reflections Appeared in Harmony With the Up and Down Oscillations
of the Liquid Metal at the Trailing Solid-Liquid Interface.

	Welding Parameters				
i_p, Amps	100	120	120	120	150
i_b, Amps	10	10	10	10	10
t_p, Sec.	0.067	0.033	0.208	0.167	0.050
t_b, Sec.	0.167	0.133	0.832	0.250	0.250
Travel, mm/sec.	2.12	2.12	2.12	4.23	2.12
	Times Between Reflections, Seconds				
1st Reflection	0.010	0.015	0.015	0.012	0.008
2nd Reflection	0.023	0.034	0.030	0.028	0.029
3rd Reflection	0.022	0.032	0.045	0.023	0.023
4th Reflection	0.021	0.033	0.045	0.022	0.023
5th Reflection	0.021	--	0.045	0.022	0.023
6th Reflection	0.022	--	0.045	0.022	0.024
7th Reflection	--	--	0.045	0.021	0.024
8th Reflection	--	--	0.045*	0.022	--

*Six more reflections were seen with 0.045 second intervals.

TABLE 2

ENERGY DISPERSIVE X-RAY ANALYSES OF

WELD SURFACE RIPPLE SPIKES AND NEARBY SPIKE FREE AREAS

Spike-Flat Area Couple	Ratio, % in Spike/% in Nearby Flat Area					
	Fe	Ni	Al	Si	Mn	Location
1	0.98	0.87	--	2.8	--	Just After $i_p \rightarrow i_b$
2	1.01	0.95	--	1.3	1.4	Just After $i_b \rightarrow i_p$
3	0.98	1.00	--	1.4	1.4	Just After $i_b \rightarrow i_p$
4	1.09	0.74	--	0.8	--	Just Before $i_p \rightarrow i_b$
5	1.02	0.94	--	0.6	--	Just Before $i_p \rightarrow i_b$
6	0.92	0.85	13.1	4.9	--	Just Before $i_b \rightarrow i_p$
7	0.67	0.46	40.0	17.4	--	Just Before $i_b \rightarrow i_p$
8	1.05	0.88	1.9	0.9	--	Midway in t_b

Nominal alloy composition, in wt.%: Fe-25.9 Ni-0.34 Mn-0.24, Si-0.012 C

Dwg. 6445A21

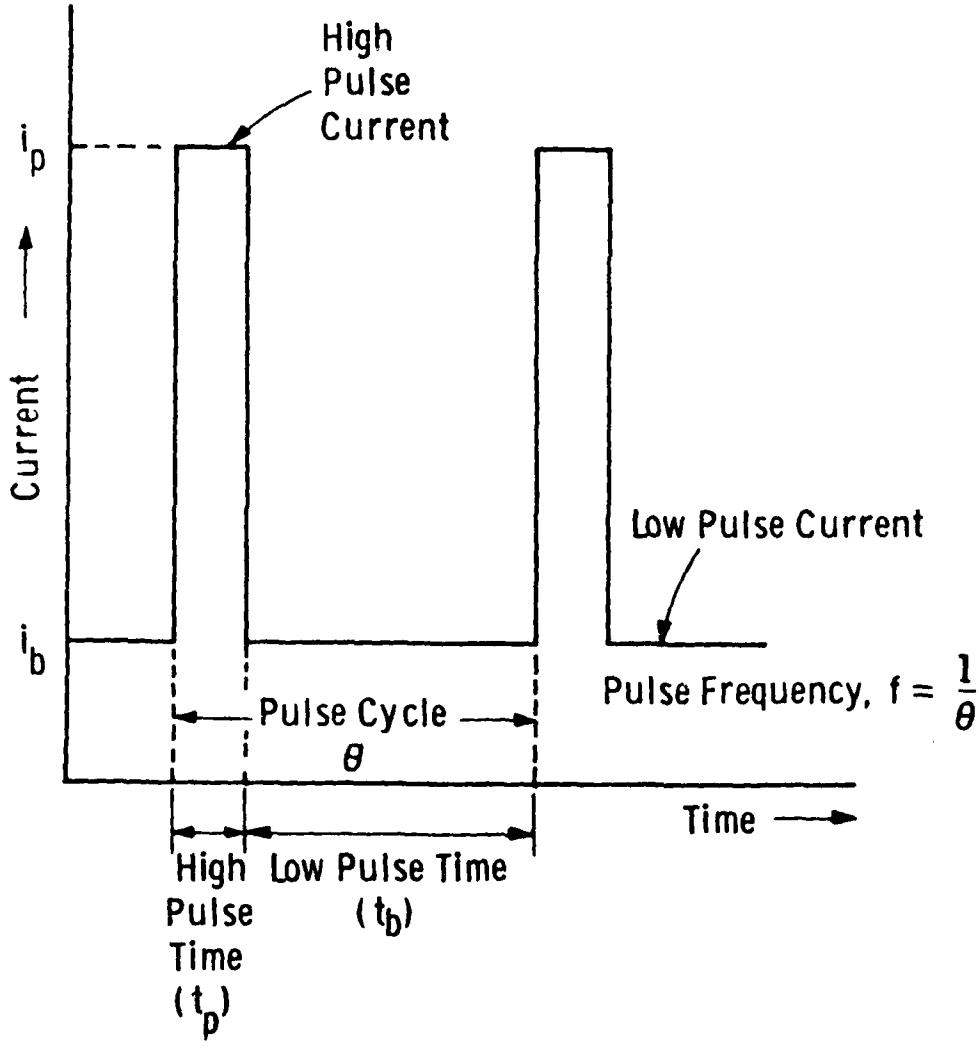

Fig. 1—An idealized pulsed current waveform and associated definitions

Dwg. 6445A22

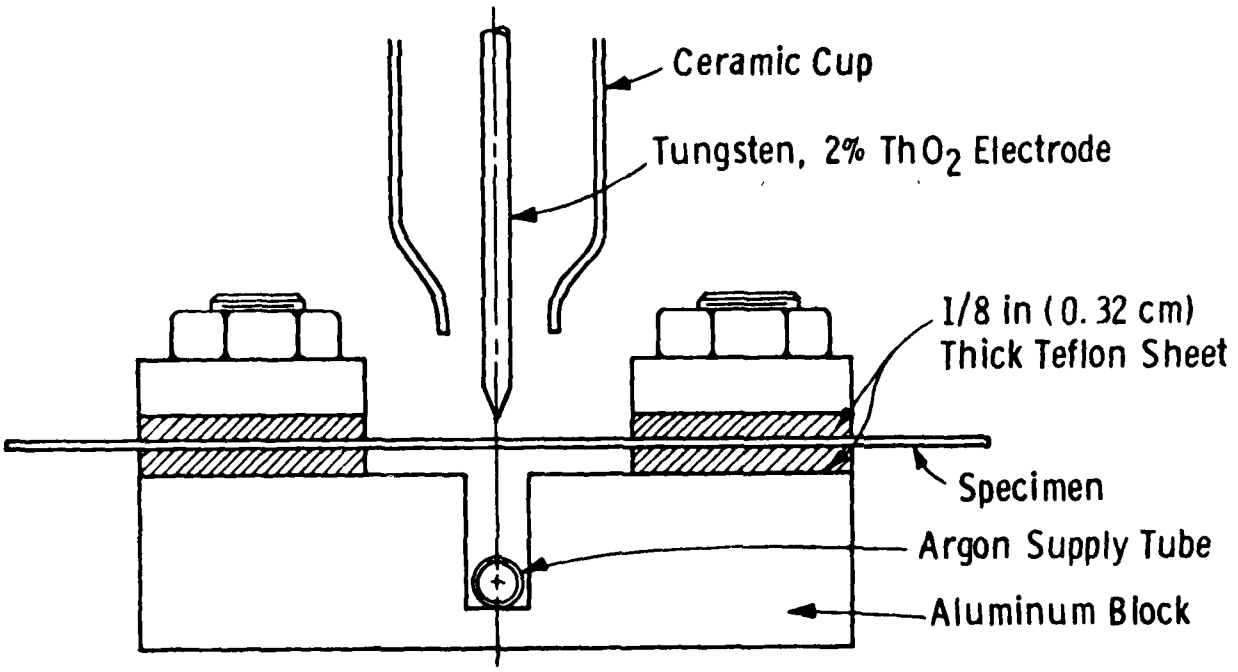

Fig. 2 —Cross-sectional view of the clamping fixture. Torch travel direction was normal to the paper

Dwg. 7735A26

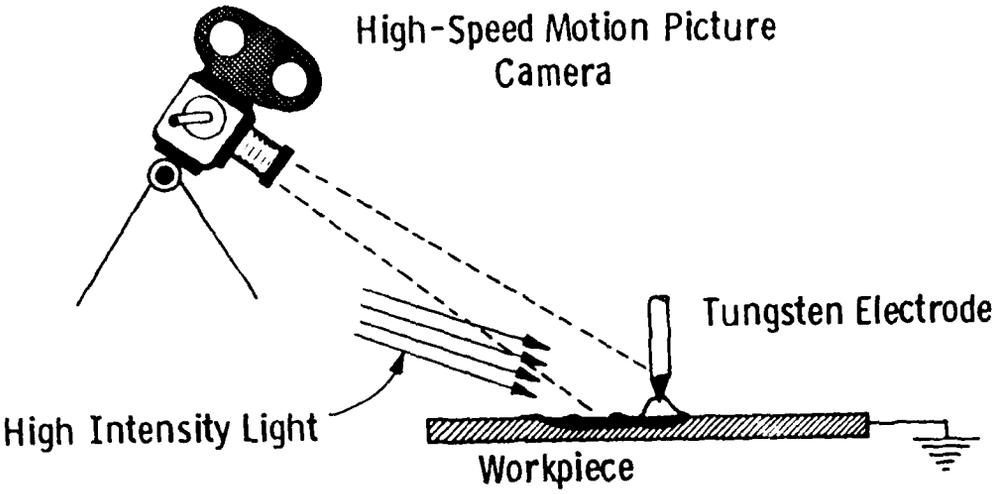

Fig. 3—Setup for high speed motion picture photography of the weld pool trailing half

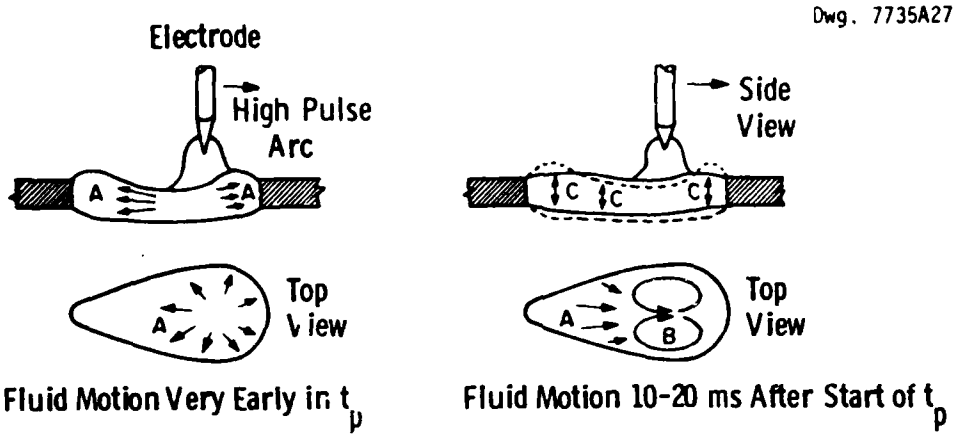

(a) Weld Pool Fluid Motion During t_p: Radially Outward and Inward (Arrows Marked (A) Rotational (B), and Up and Down Oscillating (C)

(b) Weld Pool Fluid Motion During t_b: Radial (A), Rotational (B) and Oscillating Up and Down (C)

Fig. 4—Schematics describing fluid motion in the PC-GTA weld pool at various times during a pulse cycle

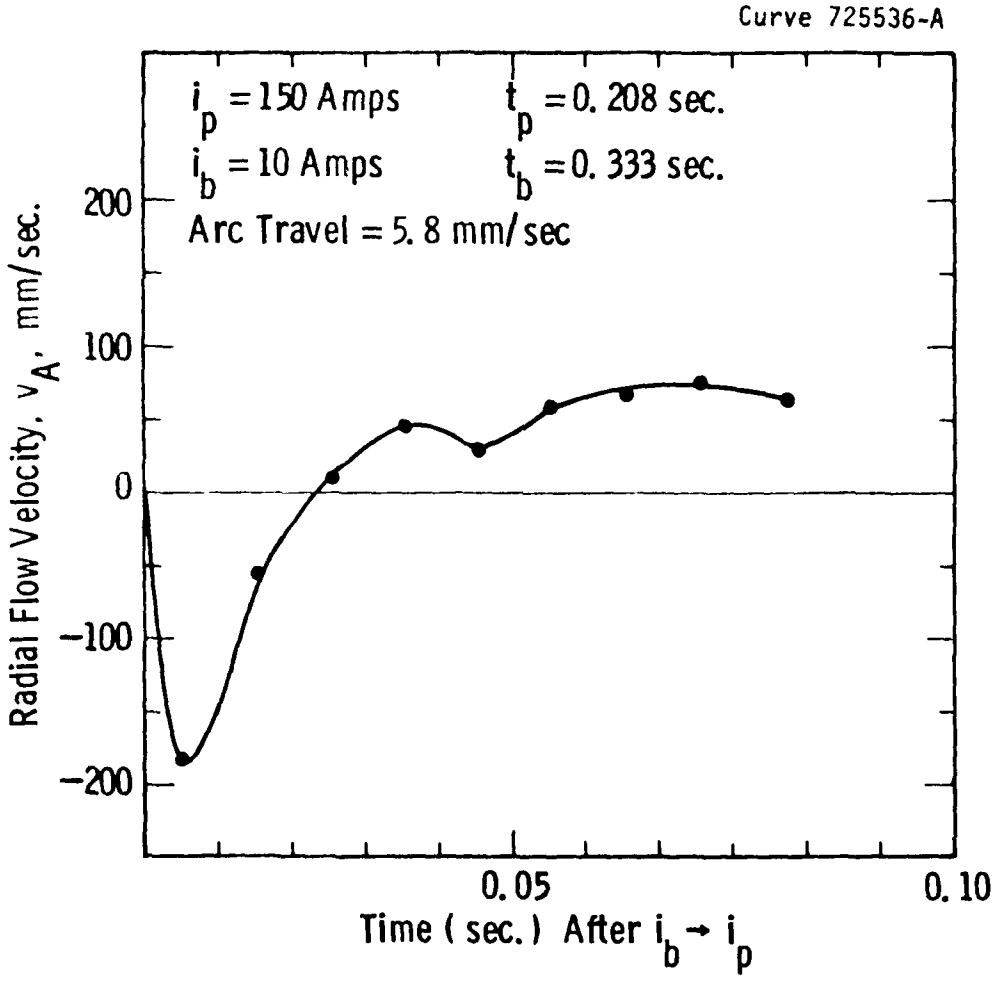

Fig. 5—Variation in speed and direction of the radial fluid flow in a PC-GTAW pool during high pulse time. Negative velocity means flow in the direction of the weld pool trailing edge

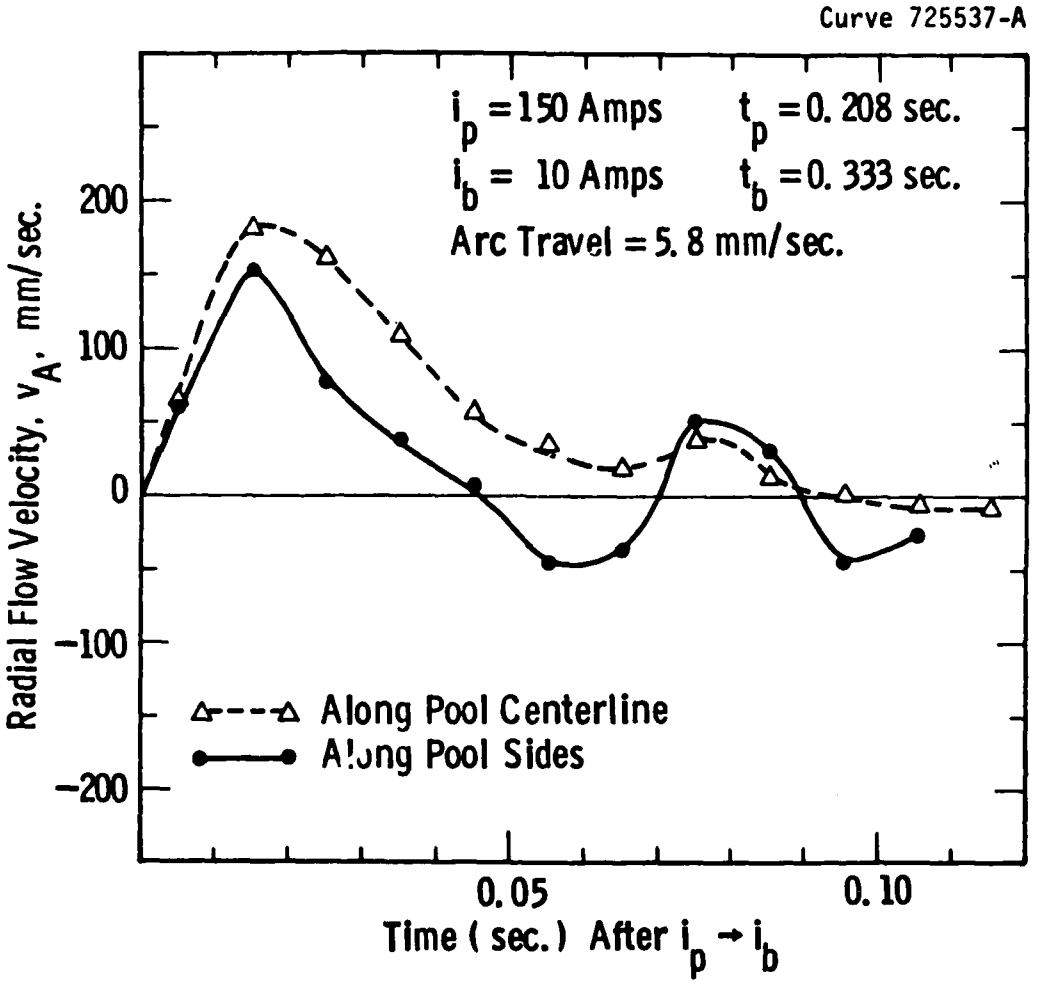

Fig. 6—Variation in speed and direction of the radial fluid flow in a PC-GTAW pool during low pulse time. Negative velocity means flow in the direction of the weld pool trailing edge

One motion picture frame prior to $i_p \rightarrow i_b$ transition.
Note weld ripples previously formed at the bottom portion of the picture.

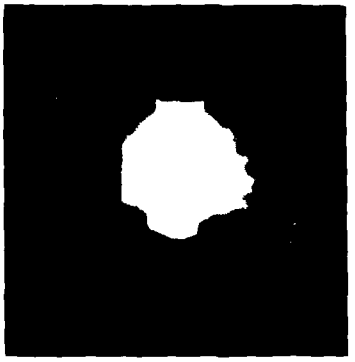

2 frames after $i_p \rightarrow i_b$

7 frames after $i_p \rightarrow i_b$

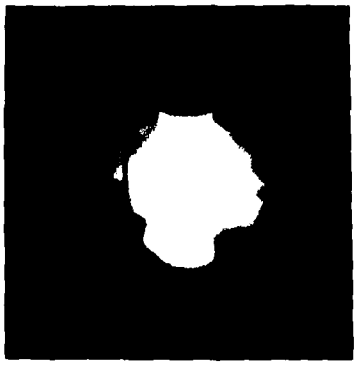

9 frames after $i_p \rightarrow i_b$

11 frames after $i_p \rightarrow i_b$

Figure 7 - A sequence of photos from a high speed (1000 frames/sec) motion picture of a pulsed current arc and its reflection in the weld pool. Formation of a wave of liquid metal by the transition from a high current (i_p) arc to a low current (i_b) arc is seen.

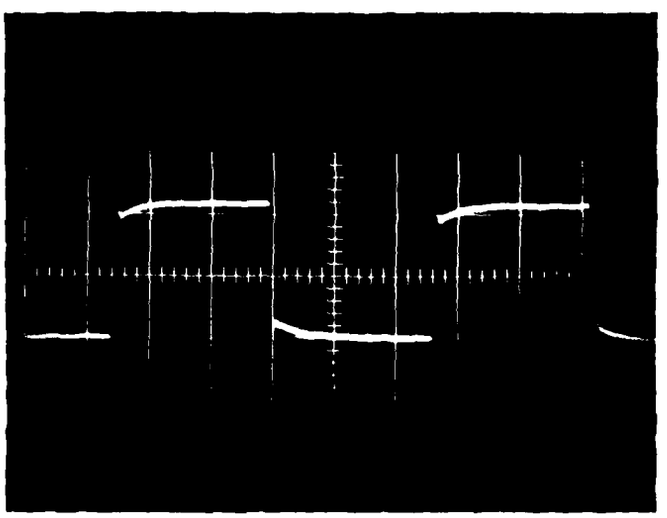

Figure 8 - Oscilloscope trace of a pulsed current waveform at 100 Hz, i_p = 120 amps and i_b = 30 amps. The units of the x-axis are 0.002 sec/cm, and the y-axis 0.01 volts/cm.

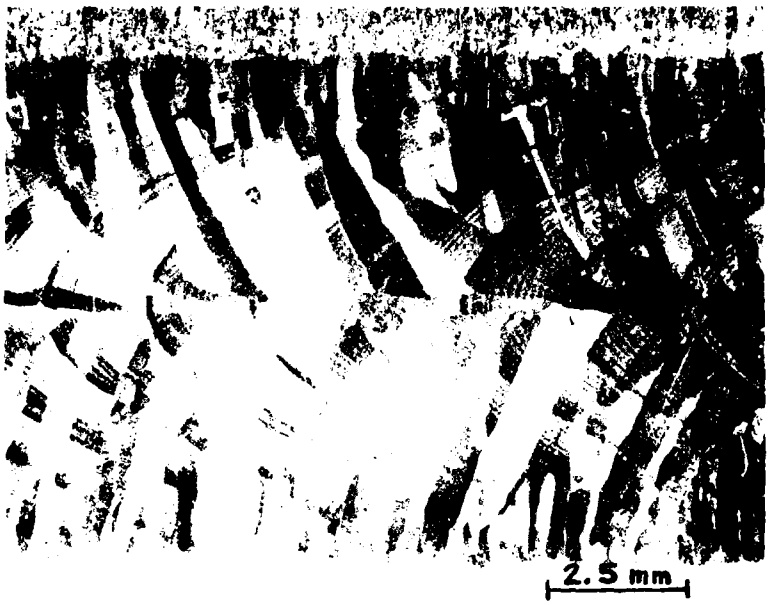

Figure 9 - Top surface of a full penetration PC-GTA weld showing typical ripples. Unetched, but solidification structure is emphasized due to slight oxidation in welding.

Figure 10 - A composite SEM micrograph showing weld surface ripples as made up of individual spikes protruding from the weld surface is pictured here. Portions solidified during t_p and t_b are identified by locating the two major ripples formed at the beginnings of these periods.

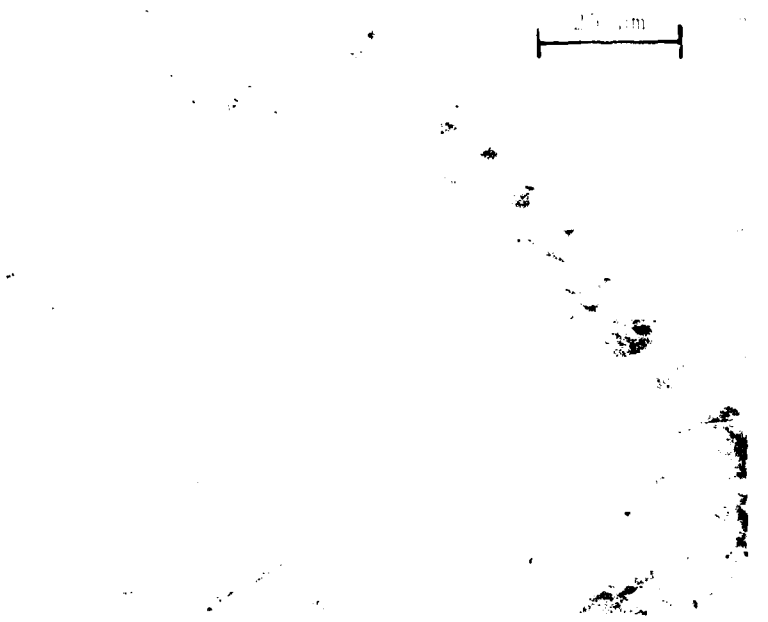

Figure 11 - An SEM micrograph of ripple spikes formed preferentially at the solidification cell boundaries.

Curve 723685-A

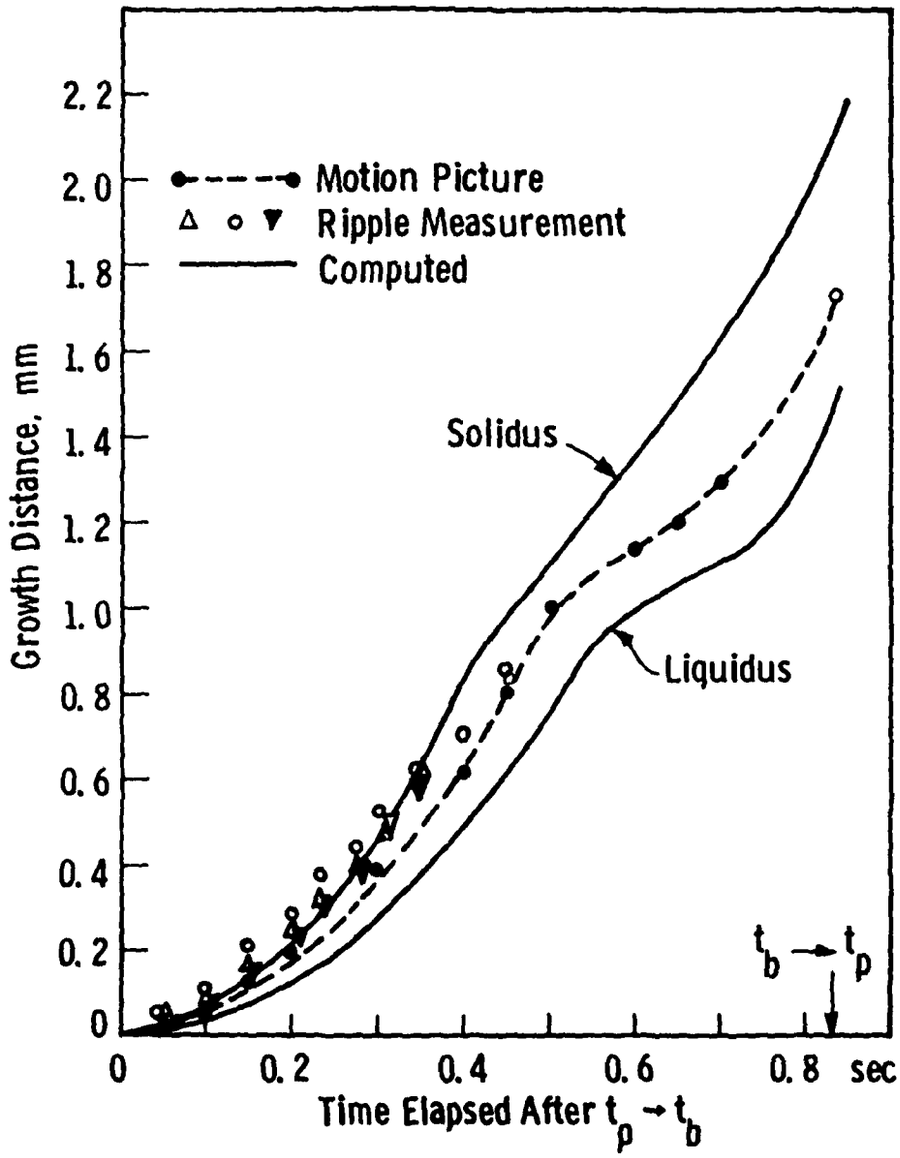

Fig. 12—A comparison of solid growth distances at the trailing edge of a weld pool ($i_p = 120$ Amps, $i_b = 10$ Amps, $t_p = 0.208$ sec., $t_b = 0.832$ sec., arc travel = 0.212 cm/sec.)

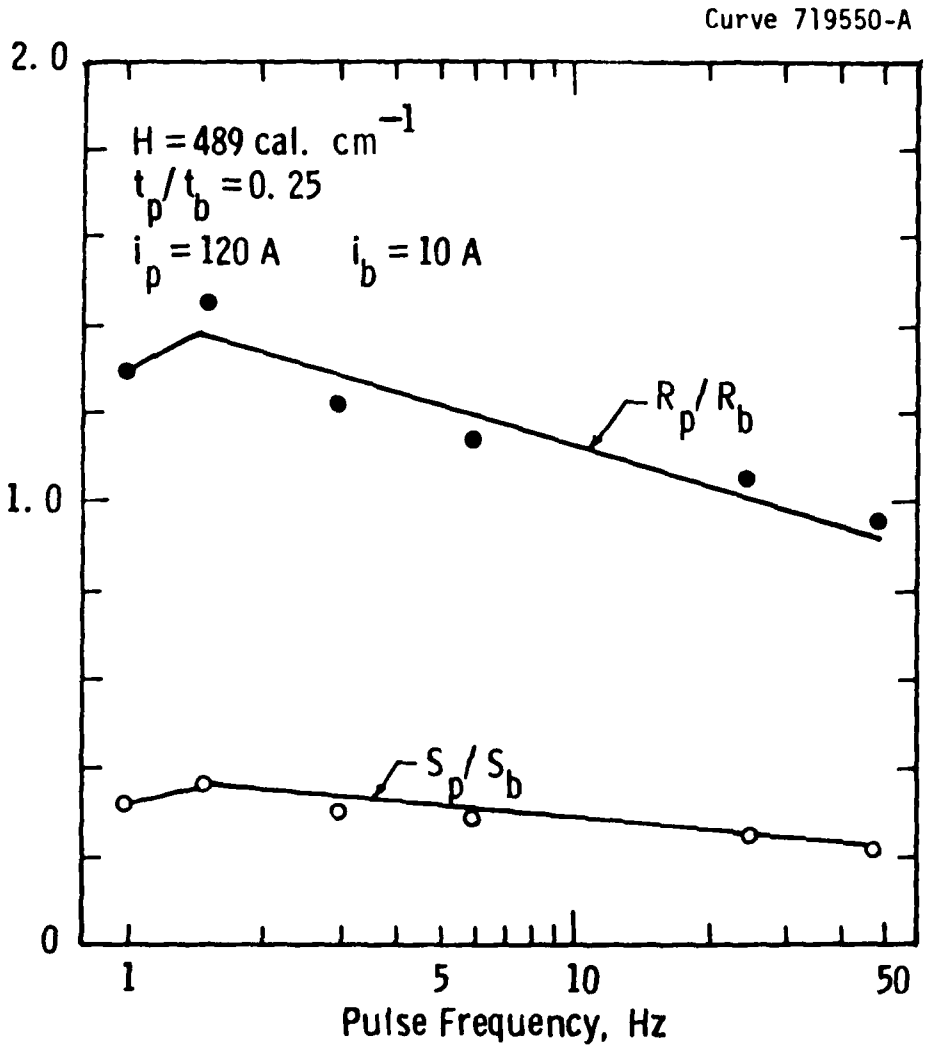

Fig. 13—Effect of pulse frequency on the ratio of solidification distances (S_p, S_b) during t_p and t_b, and the ratio of rates of solidification (R_p, R_b) during t_p and t_b for the trailing edge of the weld pool.

PART II

HEAT-FLOW SIMULATION OF PULSED CURRENT

GAS TUNGSTEN ARC WELDING

G. M. Ecer and M. Downs

Westinghouse R&D Center

Pittsburgh, PA 15235

H. D. Brody and A. Gokhale

University of Pittsburgh

Pittsburgh, PA 15261

ABSTRACT

As one aspect of a program to determine the relations among welding parameters, heat flow, weld zone structure and weld soundness in pulsed arc welding, computer simulations of the heat flow in pulsed welded sheets and plates are being developed. The results of the computer simulations are being compared to thermocouple measurements of the temperature cycles and distributions within the weldment and high speed cinematographic measurements of the variation of the size of the weld pool. The explicit finite difference technique used for the two-dimensional heat flow computations has been found adequate in predicting temperature fields, thermal gradients, the solidus and liquidus movements in and around the weld pool, as well as its size and shape.

INTRODUCTION

The technique of pulsed arc welding combines the desirable features of a high energy input rate process with the advantages of low total heat input. Practical benefits that may be achieved by pulsing include reduction of heat build-up along the weld seam[1], improved weld bead size and shape control[2], improved arc stability[3], reduced sensitivity to disparity in heat sink[2], and overcoming of the gravity effects on the weld pool. Furthermore, in controlling weld metal solidification, pulsed-current arc welding provides more parametric freedom than conventional steady-current methods. The added flexibility results from the new process variables emerging from the cycling of the arc current between high and low currents with the current waveform conforming to a variety of designs. In its simplest form, the arc current follows a square waveshape and introduces six process variables in place of two. The variables of current and voltage in steady-current welding are replaced by high pulse and low pulse currents, their durations (Figure 1) and the corresponding arc voltages. The increased complexity of the weld metal structural control resulting from the introduction of the new variables may be overcome by the utilization of computer-based heat flow simulation techniques.

As one aspect of a program to determine the relations among welding parameters, heat flow, weld zone structure and weld soundness in pulsed arc welding, computer simulations of the heat flow in pulsed welded sheets and plates are being developed. The present paper reports the results of the computer simulations of the pulsed-current GTA welding of thin sheets under two-dimensional heat flow. The predicted temperature fields around a weld pool are compared with those experimentally determined and the simulated movement of the weld pool solidification isotherms is verified through high speed cinematographic measurements.

METHODOLOGY

Computations

The heat flow simulation uses an explicit finite difference technique based on the governing relation for the two-dimensional heat flow in thin sheets

$$\rho C_p \frac{\partial T}{\partial t} = \frac{\partial}{\partial x}\left(k \frac{\partial T}{\partial x}\right) + \frac{\partial}{\partial y}\left(k \frac{\partial T}{\partial y}\right) + \frac{q}{\omega} \qquad (1)$$

where the term on the left represents the heat accumulation within a differential region of interest and the first two terms on the right represent the difference between heat conducted into and out of the differential element (per unit volume per unit time). The last term on the right is the rate of heat input into or loss from the differential region, such as heat input from the arc or heat loss by radiation or convection from the surface. q is the heat flux (per unit area per unit time) and ω is the plate thickness. k is the thermal conductivity, ρ is the density and C_p is the heat capacity of the alloy being welded.

The computational method accounts for the heat loss from top and bottom surfaces by convection and radiation through the expressions

$$q = [2h_r + h_c \text{ (top)} + h_c \text{ (bottom)}] (T - T_o) \qquad (2)$$

$$h_r = \sigma\varepsilon [T_a^2 + T_{ao}^2][T_{ao}] \qquad (3)$$

$$h_c = h' (T - T_o)^{0.25} \qquad (4)$$

where σ is the Stefan-Boltzman constant, ε is the emissivity, T_a and T_{ao} are the absolute temperature of the surface and ambient, respectively, and h' is a constant in the expression for the heat transfer coefficient for convection.

In the nodal network used, shown in Figure 2, a region of interest near the weld pool is given increased resolution by making the node spacings finer than the surrounding regions. The network itself represents one half of the sheet metal being welded, the other half is assumed the mirror image of the half shown. At the centerline (x = 0), no heat flow to the other side, or dT/dx = 0, is assumed. The rows and columns of the network are numbered as:

Small grid rows	$1 < J < n$
Small grid columns	$1 < I < m$
Large grid rows	$1 < K < N$
Large grid columns	$1 < L < M$

where n, m, N and M are 72, 22, 85 and 22, respectively, in the version of the computer program whose results are reported here.

The nodal difference equation written for equal increments in x and y within an internal element in the large grid becomes

$$T'_{K,L} = T_{K,L} + \phi \left[T_{K+1,L} + T_{K-1,L} + T_{K,L+1} + T_{K,L-1} - 4T_{K,L} + 8/k\omega\right] \quad (5)$$

T' and T are the nodal temperatures at $t + \Delta t$ and t, respectively,

$$\phi = \frac{\alpha \Delta t}{\Delta X^2} \quad (6)$$

$$\alpha = \frac{k}{\rho Cp} \quad (7)$$

and ΔX is the node spacing. The node spacing is uniform within the two regions and the spacings differ by any, preselected, integral factor. The time step in the explicit finite difference analysis is limited by

$$\Delta t < \frac{\Delta X^2}{2\alpha s} \quad (8)$$

where s = the number of dimensions in the analysis.

The contribution of weld pool convection is incorporated into the computations by multiplying the conductivity of the liquid by a factor ranging from 3 to 10. In order to conserve computer time, three zones are set up and a different time step is used in each. In the region with the large node spacing (region 1) a large time step is used. The grid with small node spacing is divided into two zones. The region containing the liquid zone (region 3) is given the largest number of iterations and the smallest time step (due to its small spacing and high assumed thermal conductivity). The rest of the small grid region (region 2) receives an intermediate number of iterations. In the limit the time steps are related by

$$\Delta t_1 = a^2 \Delta t_2 = a^2 b \Delta t_3 \tag{9}$$

where a = ratio of the node spacings, and b = the factor used to increase the thermal conductivity.

The heat input from the arc is spread over several nodes, usually eight. The amount of heat input to each node is weighted and the weighting is changed after each iteration of the time step for region 2 to simulate the movement of the arc. Whenever the arc would have moved the distance of one large node spacing, all nodes are renumbered. The heat input to a node from the arc is calculated by

$$q_p = \frac{1}{4.18} \quad w\mu \; i_p \; e_p \quad \text{(cal/sec)}$$

$$q_b = \frac{1}{4.18} \quad w\mu \; i_b \; e_b \tag{10}$$

where w = weighting factor for the node,

μ = welding arc heat transfer efficiency,

i_p, i_b = arc current for peak and background pulses, respectively,

e_p, e_b = arc voltage for peak and background pulses, respectively.

At the far edges of the simulated sheet heat transfer is assumed to continue in a way to keep a constant curvature for the T vs. x curve,

or for $T_{K,M}$ at $x = (M-2)\Delta x$

$$\frac{T_{K,M} - T_o}{T_{K,M-1} - T_o} = \frac{T_{K,M-1} - T_o}{T_{K,M-2} - T_o} \tag{11}$$

A simplified flow diagram for the computer program simulating the pulsed arc welding is shown in Figure 3. A more detailed description of the finite difference method used to approximate heat flow in pulsed current welding was given elsewhere[4]. The input data includes such welding parameters as heat input during t_p and t_b, arc travel speed and values of t_p and t_b and material related properties including solidus and liquidus temperatures, k, ρ, and C_p values for solid, liquid and mushy alloys. Single values for α, k and C_p, selected near the melting point of the alloy, were used in the computations, although they could be introduced as functions of temperature. The latter, however, would have increased the computer time while adding little to the accuracy of the results for the weld pool vicinity which is the zone of interest from the solidification point of view.

The literature sources and the manner of estimating these material properties for the Fe-26Ni alloy used in the present investigation were provided in a previous paper[5]. The material properties used in the computations reported herein are given in Table 1.

Initial temperatures $T_{K,L}$ and $T_{J,I}$ are established by setting them equal to T_o (25°C in most runs). The computer is asked to repeatedly calculate the new times and temperatures until at least 14 seconds elapse. By this time, as experiments indicate, weld size reaches a steady state. Thermal gradients weld pool boundaries and interface velocities may be computed, and time, temperature and position prints for the entire nodal network may be obtained. As a quick check of the size and shape of the weld pool and the temperature field around it printer plots of the melt zones (regions 2 and 3) may be produced. Figure 4 is one such printer plot

where isothermal lines are indicated as boundaries between two adjacent number regions, the mushy zone is shown by (+) signs and the liquid pool is indicated by the (*) signs. The arc position is shown by the four A's.

Experimental

Figure 5 is a schematic of the clamping fixture used to make full penetration welds in 0.08 cm thick sheets of the Fe-26Ni alloy. The welding parameters used for the welds discussed in this paper are listed in Table 2. The tungsten arc moved normal to the plane of the sketch in the direction of the ground connection. The arc length was kept constant at 0.1 in. (0.25 cm). The use of Teflon, with a thermal conductivity of about 250 times less than that of the Fe-26Ni alloy, was to assure two dimensional heat removal from the weld zone.

In addition to the above, the following parameters were kept constant: electrode composition, size and shape were W + 2% ThO_2, 1/8 in. (0.32 cm) diameter, 30° included vertex angle with 0.04 in. (0.1 cm) diameter flat tip; 100% argon as shield gas flowing at a rate of 40 cfh (18.9 ℓ/min) from around the electrode and 4 cfh (1.9 ℓ/min) o the back of the weldment; electrode stick-out from the cup 0.5 in. (1.25 cm) and from the collet 1.16 in. (2.95 cm). All welding was done with direct current electrode negative. Pulsed current waveform remained nearly square shaped within the pulse frequency range of 1 to 100 Hz; an example is shown in Figure 6.

Temperature measurements were taken using 0.02 cm diameter Pt-Pt + 10% Rh thermocouples placed close to and within the fusion zone on the underside of the weldment. The thermocouples were tack welded to the sheet. The thermocouple output was recorded on light sensitive paper using a high speed multi-channel recorder. Arc current transitions from high to low (or vice versa) pulse currents were automatically and instantly marked by the recorder.

High speed motion picture observations of weld pools from the trailing edge direction and from the side were made when the weld puddles reached a steady size. The camera speed increased to about 1000 frames/sec. after the first 0.3 seconds of operation. A pulsating red light within the camera provided markers on the film at a rate of 100 markers per second for more precise measurements of the camera speed. The films produced were analyzed using a professional editing machine with the capacity to record lapsing time and frame sequence electronically. Films were viewed at various speeds as well as frame by frame.

RESULTS AND DISCUSSION

In pulsed welding cycling of the arc current between i_p and i_b and the resulting cyclic variation in heat input can have pronounced effects on the weld geometry. This is illustrated in Figure 7 where the surface appearances of a steady current weld and a pulsed current weld are compared. The bottom macrograph is that of the pulsed current weld No. M1 (Table 2) where the pitch, equal to the product of the travel speed and pulse period, was long (P = 3.0 mm) so that the weld appeared as a series of superimposed spot welds. With extremely large pitch, the pool could solidify completely between peak pulses. Smaller pitched pulsed welds, too, could solidify between peak pulses under conditions of low arc speed and large t_b/t_p ratio, thus allowing time to dissipate heat. On the other hand, short pitch and small t_b/t_p ratio pulsed welds would appear and behave as continuous welds.

Temperature cycles experienced by a point within or near the weld zone depends on the sum effect of a number of welding process and material variables that include i_p, i_b, t_p, t_b, arc travel speed, k, α, as well as the distance from the weld centerline. When full penetration welds are desired, under two dimensional heat flow conditions, weld bead width on top and bottom surfaces of the workpiece should be approximately

equal. Except for the weld No. L6, all of the welds listed in Table 2 could be considered as 2-D welds, since all showed top to bottom bead width ratios higher than 0.93. In making 2-D welds in thin sheets, one is restricted to a critical maximum heat input per unit length, for a given sheet thickness, above which weld pool surface tension is not sufficient to hold the weld metal together and a weld metal "drop-through" occurs. Thus, all of the process variables have upper and lower limits. Under even such limitations, temperature cycling at points near the weld fusion line can be quite varied and substantial as exemplified by the experimental and computational results presented below.

The temperature vs. time plots of Figures 8 and 11 present the results of computer simulations of the experience of selected locations in the workpiece in comparison with those determined by thermocouple measurements for similar locations. Figure 8 is for a steady current weld; Figures 9-11 are for pulsed current weld. In Figures 8 and 11 the position of the thermocouple locations is displaced slightly from the location of the computer simulation. The locations in Figure 12 were within fusion zone and the thermocouple failed on approach of the arc. The tendency for the experimental temperature plots, for the pulsed current welds, to show somewhat depressed temperature cycling may be a result of the slow response of the thermocouples to sudden changes in temperature. In all four cases computed temperatures are remarkably close to the measured temperatures.

The magnitude of the temperature fluctuations in the liquid and at the interface (mushy zone) may have a bearing on any possible grain multiplication and structure modification that may result from dendrite remelting. In the present study, all of the welds under discussion showed predominantly cellular-columnar solidification structures with small tendency to form dendritic-columnar growth in long pitched, low heat input welds. As a consequence, none of the welds exhibited any degree of equiaxed grain formation. Under three dimensional heat flow conditions for pulsed

welding of thicker plates of the Fe-26Ni alloy and a stainless steel, however, some grain refining effect due to arc current pulsing could be obtained as has been reported elsewhere[6,7].

The computer model predictions of the variations in the weld pool area (A_M), the mushy zone area (A_{MZ}) and length and width of the weld pool within a single pulse period are for a typical pulsed weld shown in Figure 12. The maxima in weld pool width, weld pool length, and weld pool area may be measured from the ripple formation on the weld surface. These three measurements for weld J7 are compared to the maxima on the computed curves. Again, agreement is remarkably good.

As the weld pool expands and contracts within a pulse period, cyclic increases and decreases occur in the thermal gradients along the two major axes as shown for the same weld (No. J7) in Figure 13. The relative constancy of the thermal gradient along the trailing edge is in contrast to the more greatly varying gradient in the transverse direction. It has been noted, elsewhere, freezing rate in the trailing and transverse directions show similarly contrasting behavior[6,7].

The movement of the solidus and the liquidus isotherms can be simulated by the computer anytime during the course of the welding operation. An example of this is shown in Figure 14 where the solidus and the liquidus movements within a single low pulse period, after about 15 seconds of welding, have been plotted. The computed curves are compared to the high speed motion picture observations where the single curve is that perceived by the observer to be a "solid-liquid interface" since the mushy zone boundaries were too diffuse for identification. The graphs, therefore, illustrate the ability of the computational approach in providing detailed information, in this case, more detailed than that obtained through high speed motion picture observations.

SUMMARY AND CONCLUSION

A simulation of the pulsed current gas tungsten arc welding of thin sheets of the Fe-26Ni alloy was made. The explicit finite difference technique used for the two-dimensional heat flow computations has been found adequate in predicting temperature fields, thermal gradients, the solidus and the liquidus growth rate in and around the weld pool, as well as its size and shape at anytime during the course of the welding operation. The simplifying assumptions made by selecting constant values for the relevant material thermal properties did not seem to have had a major impact on the accuracy of the computed results as determined by comparisons with experimental findings.

ACKNOWLEDGMENT

This work is being sponsored by the Office of Naval Research, Metallurgy Program, Contract N00014-77-C-0596, Dr. Bruce MacDonald, Scientific Officer.

REFERENCES

1. Boughton, P., "The Pulsed TIG-Welding Process - Part 2 - Potential Applications", in Pulsed TIG Welding Seminar Handbook, Brit. Welding Institute (1973).

2. Needham, J. C., "Pulsed Current Tungsten Arc Welding", in Pulsed TIG Welding Seminar Handbook, Brit. Welding Institute (1973).

3. Ecer, G. M., "Magnetic Deflection of the Pulsed Current Welding Arc", Welding Journal, 59 (6) June 1980, Research Suppl., pp. 183-s to 191-s.

4. Brody, H. D. and Stoehr, R. A., "Computer Simulation of Heat Flow in Casting", Journal of Metals, 32 (9) September 1980, pp. 20-27.

5. Tzavaras, A., Vassilaros, A., Brody, H., and Ecer, G., "Effect of Welding Parameters on Solidification Structures in Pulsed GTA Welded Fe-26%Ni", in Physical Metallurgy of Metal Joining (Eds. R. Kossowsky and M. E. Glicksman), TMS-AIME Conf. Proceedings, 1980, pp. 82-116.

6. Gokhale, A., Brody, H., and Ecer, G., "Relation of Weld Parameters, Heat Flow and Microstructure in Pulsed GTA Welds of 321 Stainless Steel", presented at the ASM Materials and Processes Congress, Oct. 30, 1980, Cleveland, OH.

7. Gokhale, A., "Weld Pool Solidification Structure and Property Control in Pulsed Current Gas Tungsten Arc Welding", M.S. Thesis, Metallurgical Engineering, University of Pittsburgh, 1980.

TABLE 2

PULSED CURRENT GAS TUNGSTEN ARC WELDING PARAMETERS

USED TO MAKE FULL PENETRATION WELDS IN 0.08 cm THICK SHEETS

OF Fe-26Ni ALLOY

Weld No.	i_p (Amp.)	i_b (Amp.)	t_p (sec.)	t_b (sec.)	Arc Travel (cm/sec.)
G5	140	10	0.167	0.667	0.212
H8	I = 40 Amps, Steady Current				0.212
J4	120	10	0.033	0.133	0.212
J7	120	10	0.208	0.832	0.212
L6	120	10	0.167	0.333	0.605
L8	150	10	0.167	0.333	0.605
M1	150	10	0.038	0.250	0.212

TABLE 1

PROPERTIES OF THE Fe-26Ni ALLOY USED IN COMPUTATIONS

	Symbol	Units	Value
Solidus Temperature	--	°C	1443
Liquidus Temperature	--	°C	1468
Density	ρ	$g.cm^{-3}$	7.88
Thermal Conductivity	k	$cal.s^{-1}.°C^{-1}.cm^{-1}$	0.1250
Heat Capacity (Solid)	C_p	$cal.g^{-1}.°C^{-1}$	0.1427
Heat Capacity (Liquid)	C_p	$cal.g^{-1}.°C^{-1}$	0.1427
Thermal Diffusivity	$\alpha \left(=\frac{k}{C_p.\rho}\right)$	$cm^2.s^{-1}$	0.1111
Heat Capacity (Mushy Zone)	$C_p(mz)$	$cal.g^{-1}.°C^{-1}$	3.6880

Dwg. 6445A21

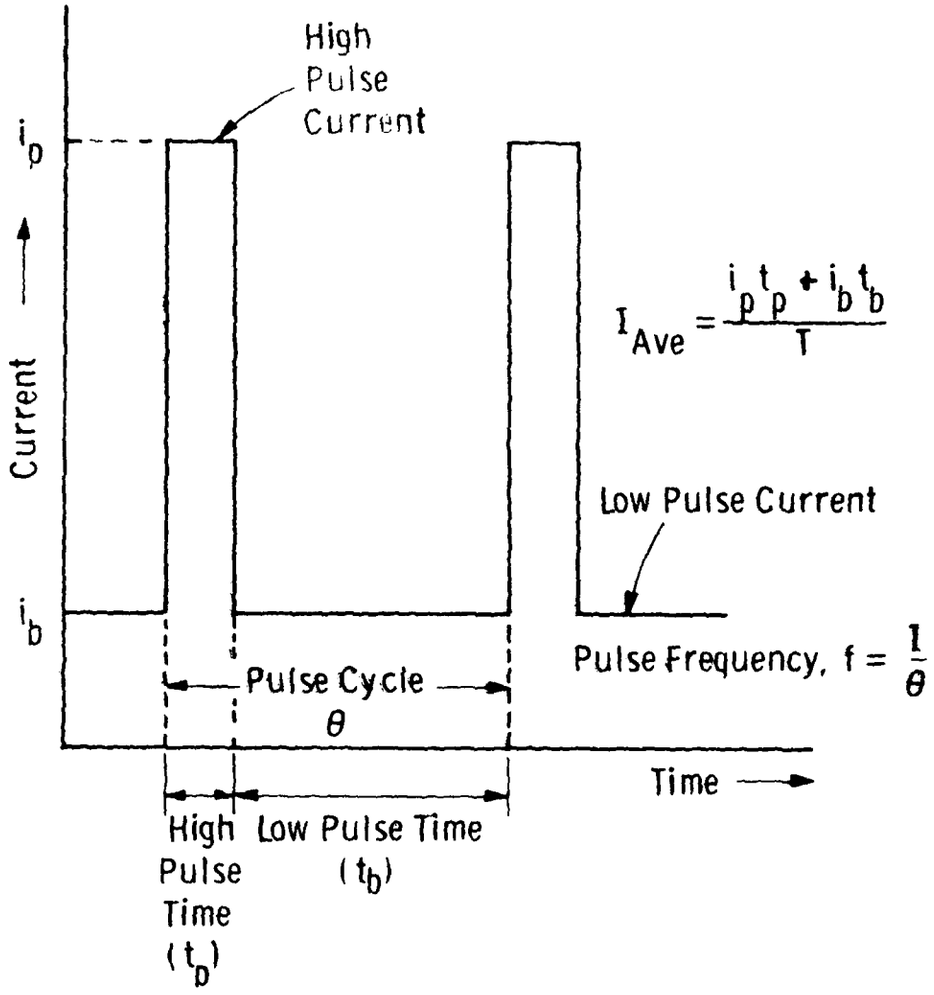

Fig. 1—An idealized pulsed current waveform and associated definitions

Dwg. 7737A82

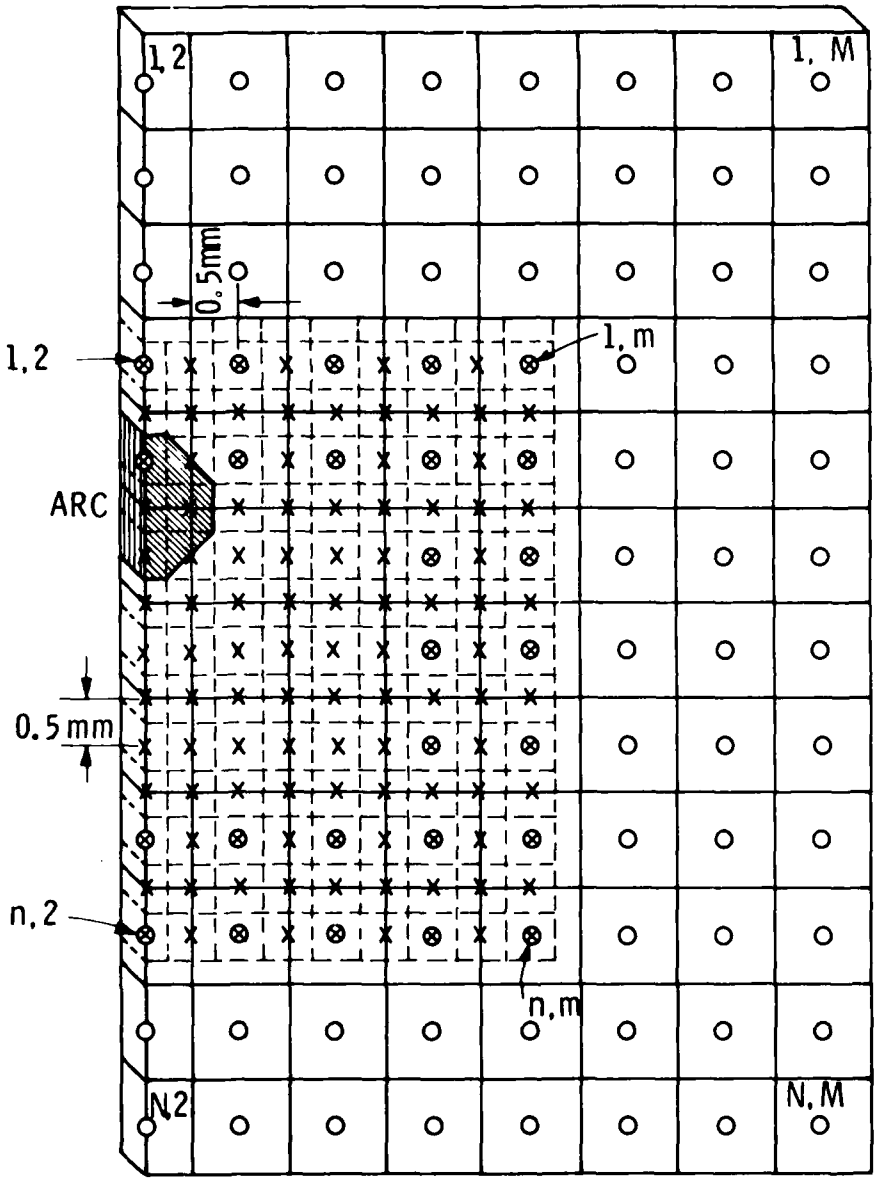

Fig. 2 — A sketch of the element mesh used for simulation of pulsed current tungsten arc welding of sheets

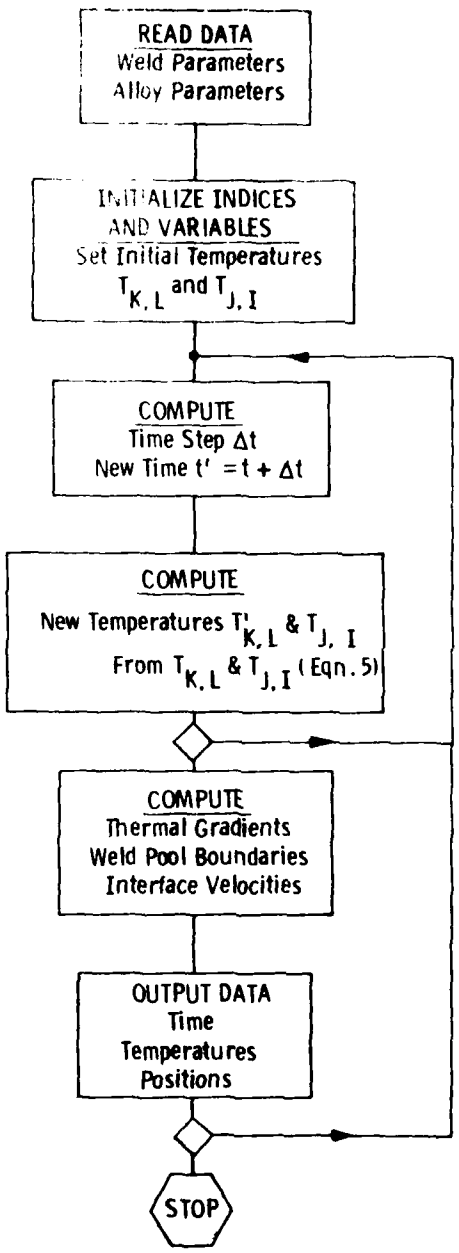

Fig. 3 – Simplified flow diagram for finite difference analysis of pulsed current arc welding

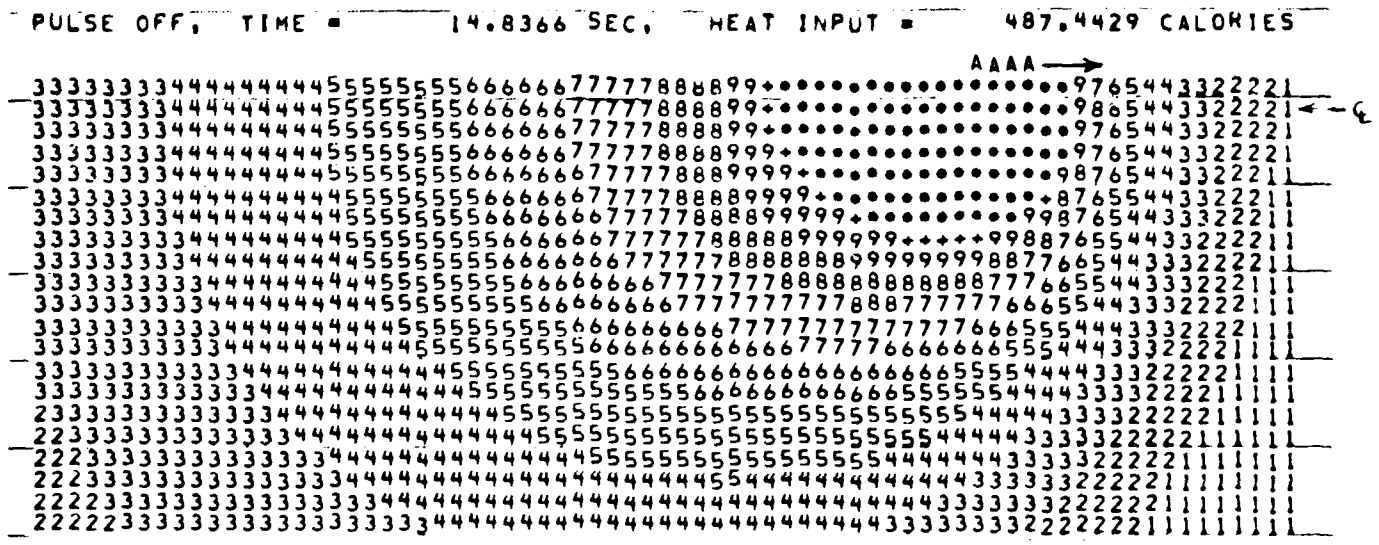

Figure 4 - A typical printer plot of the temperature zones and isothermal lines near the weld pool 14.8366 sec. after the start of the weld No. M1. Each number represents temperatures more than the product of the number and 1/10th of the melting temperature (1468°C) of the alloy. The star and plus signs indicate liquid and mushy zones respectively. Distance between points is 0.5 mm.

Dwg. 6445A22

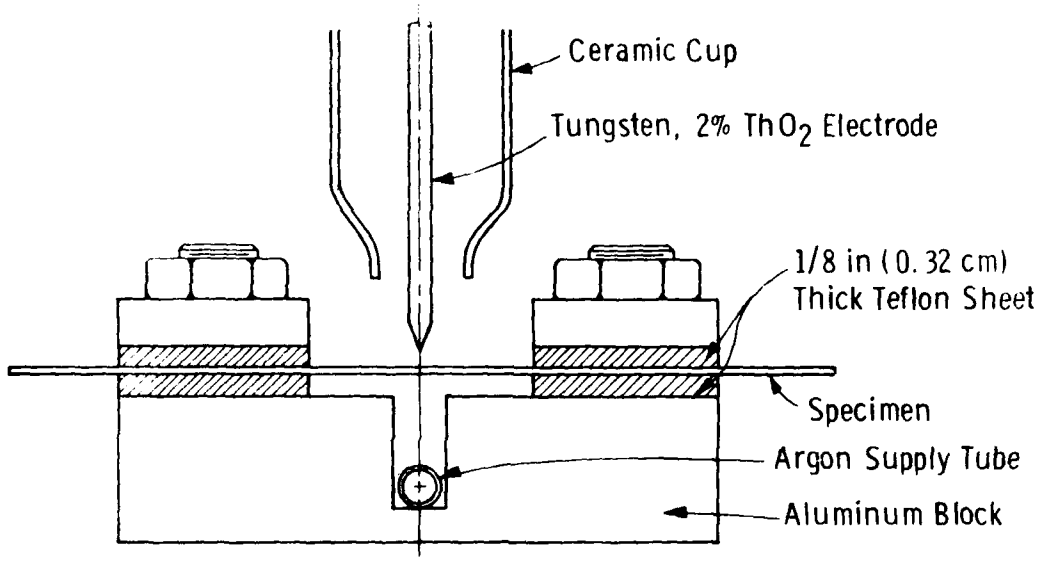

Fig. 5 —Cross-sectional view of the clamping fixture. Torch travel direction was normal to the paper

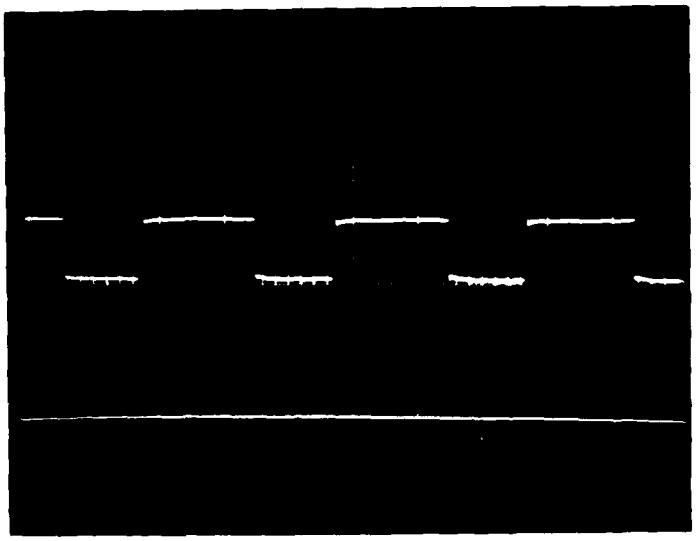

Fig. 6 – A pulsed current waveform typical of those utilized in this study. Here the pulsing parameters were:

$i_p = 150\,A$
$i_b = 25\,A$
$t_p = 0.009\,s$
$t_b = 0.006\,s$

Weld No. H8

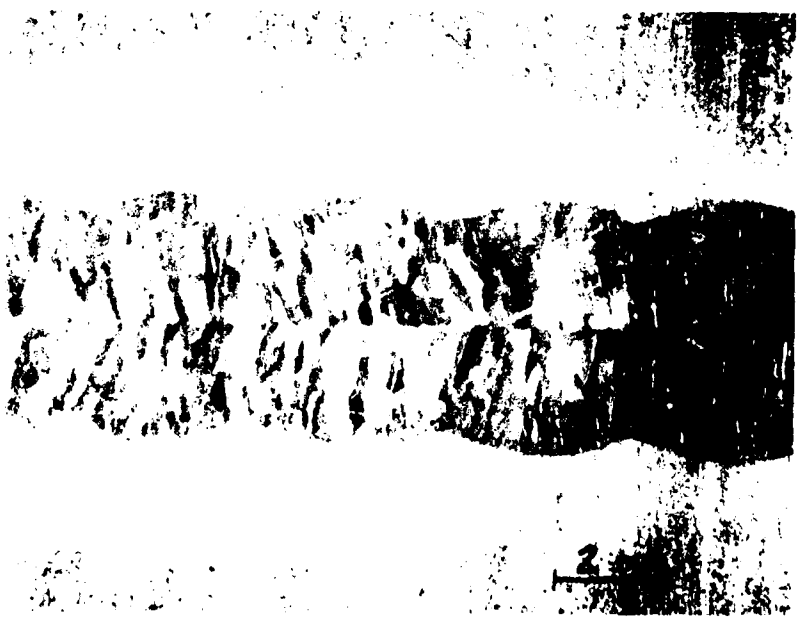

Weld No. L6

Figure 7 - Macrographs comparing the top surfaces of a steady current weld (top) and a pulsed current weld (bottom).

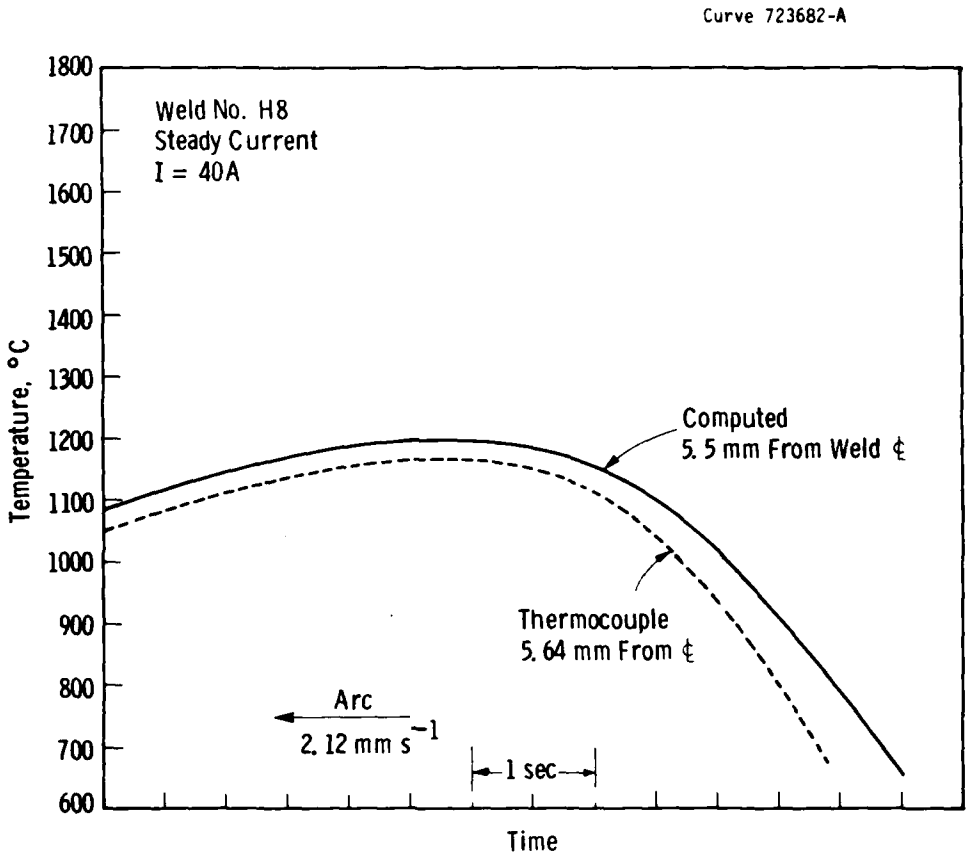

Fig. 8 — Temperature history of a point in the parent metal near the fusion line of a steady current weld. Computed and measured curves are compared. Note the slight difference in distance of the compared locations from the weld centerline

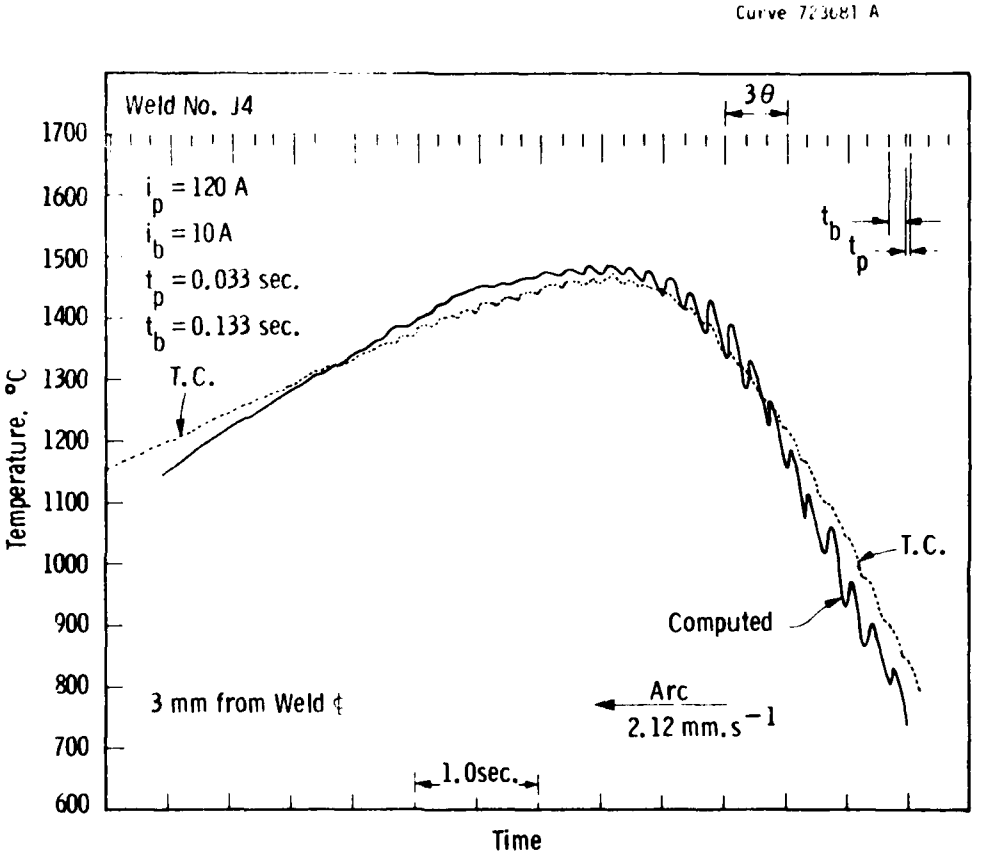

Fig. 9 — Time-temperature profile for a point just within the fusion zone of a pulsed current weld of relatively short pitch (P = 0.35 mm)

Curve 723683-A

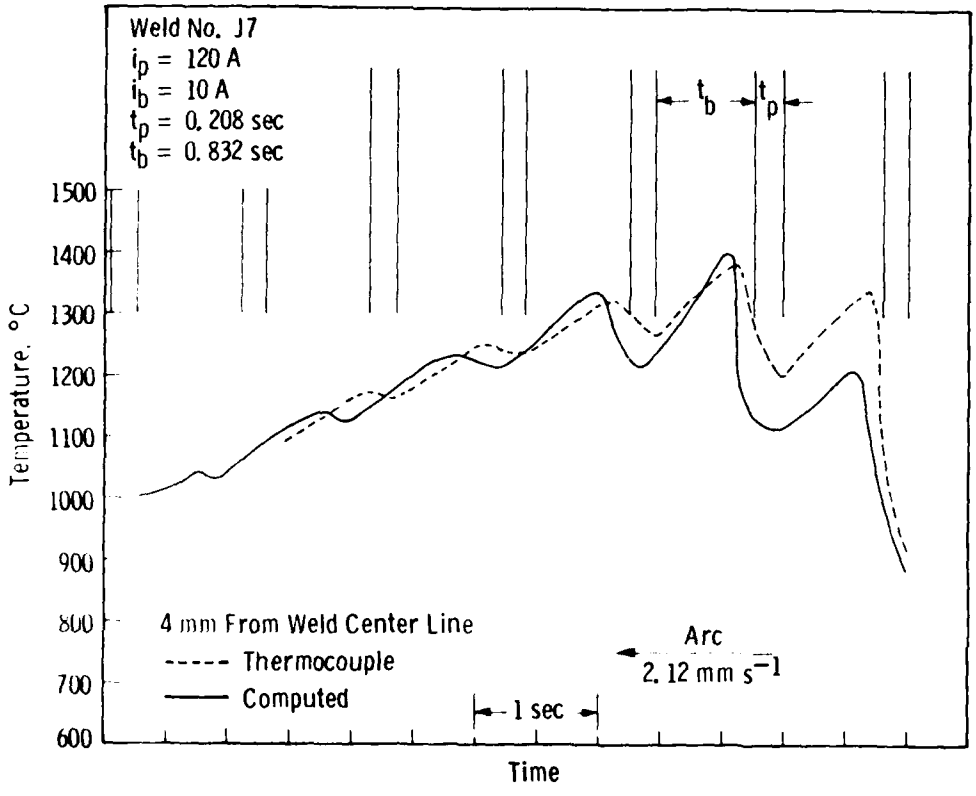

Fig. 10 — Time-temperature profile for a point in the parent metal near the fusion line of a pulsed current weld of moderate pitch (P = 2.2 mm)

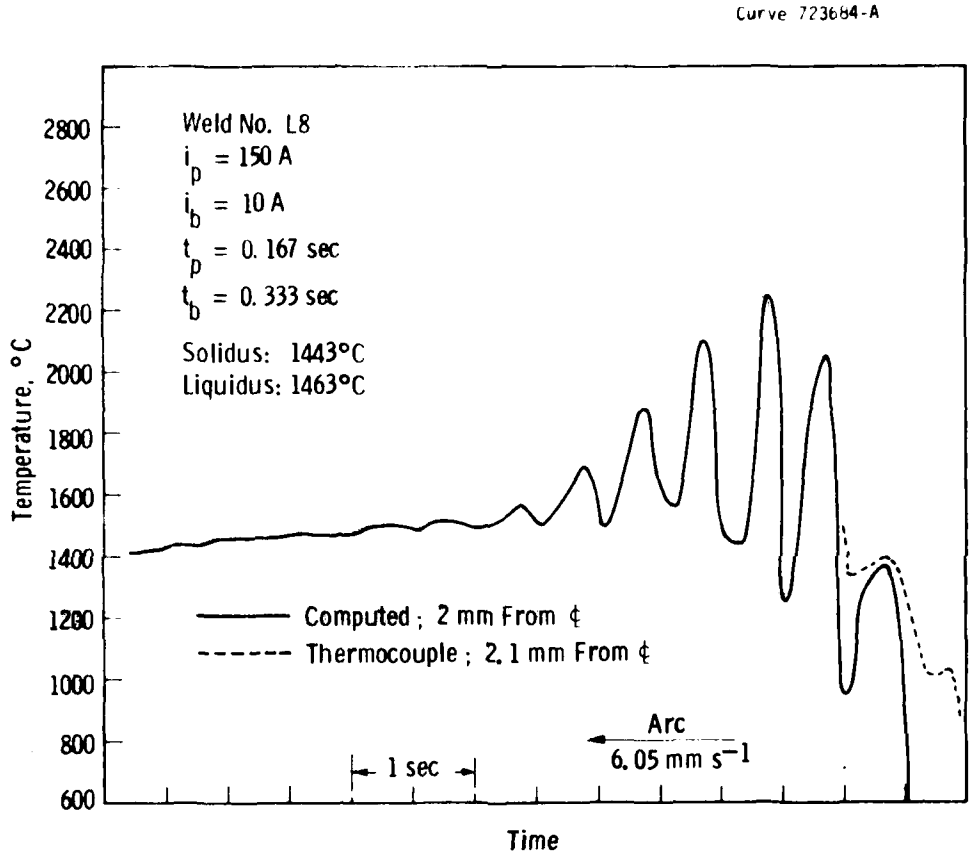

Fig. 11 – Time-Temperature profile for a point in the fusion zone of a pulsed current weld of moderately long pitch (P = 3 mm) . Note the thermocouple malfunction in the melt zone

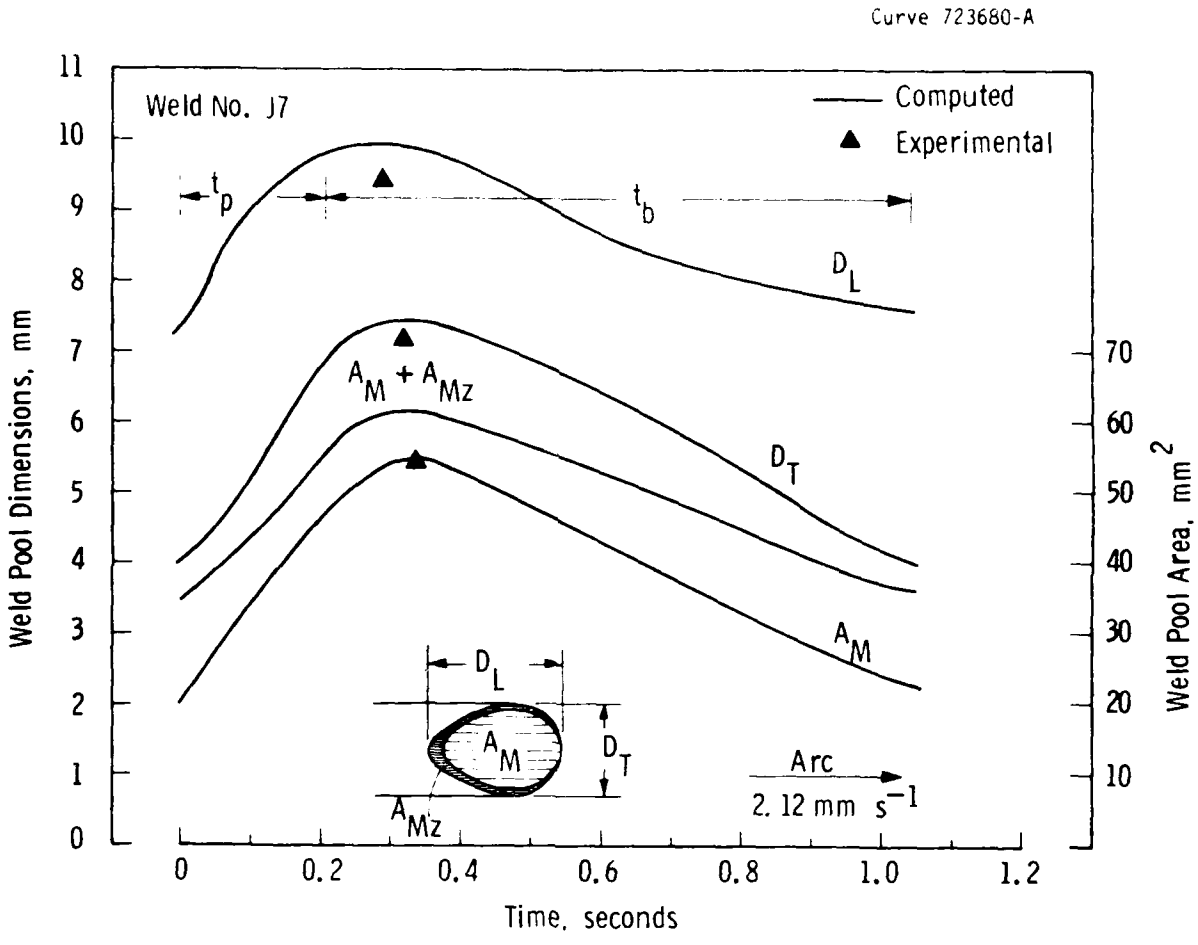

Fig. 12 – Variations of the weld pool length (D_L), width (D_T), mushy zone (A_{MZ}) and the size of the liquid pool within a pulse period

Curve 723679-A

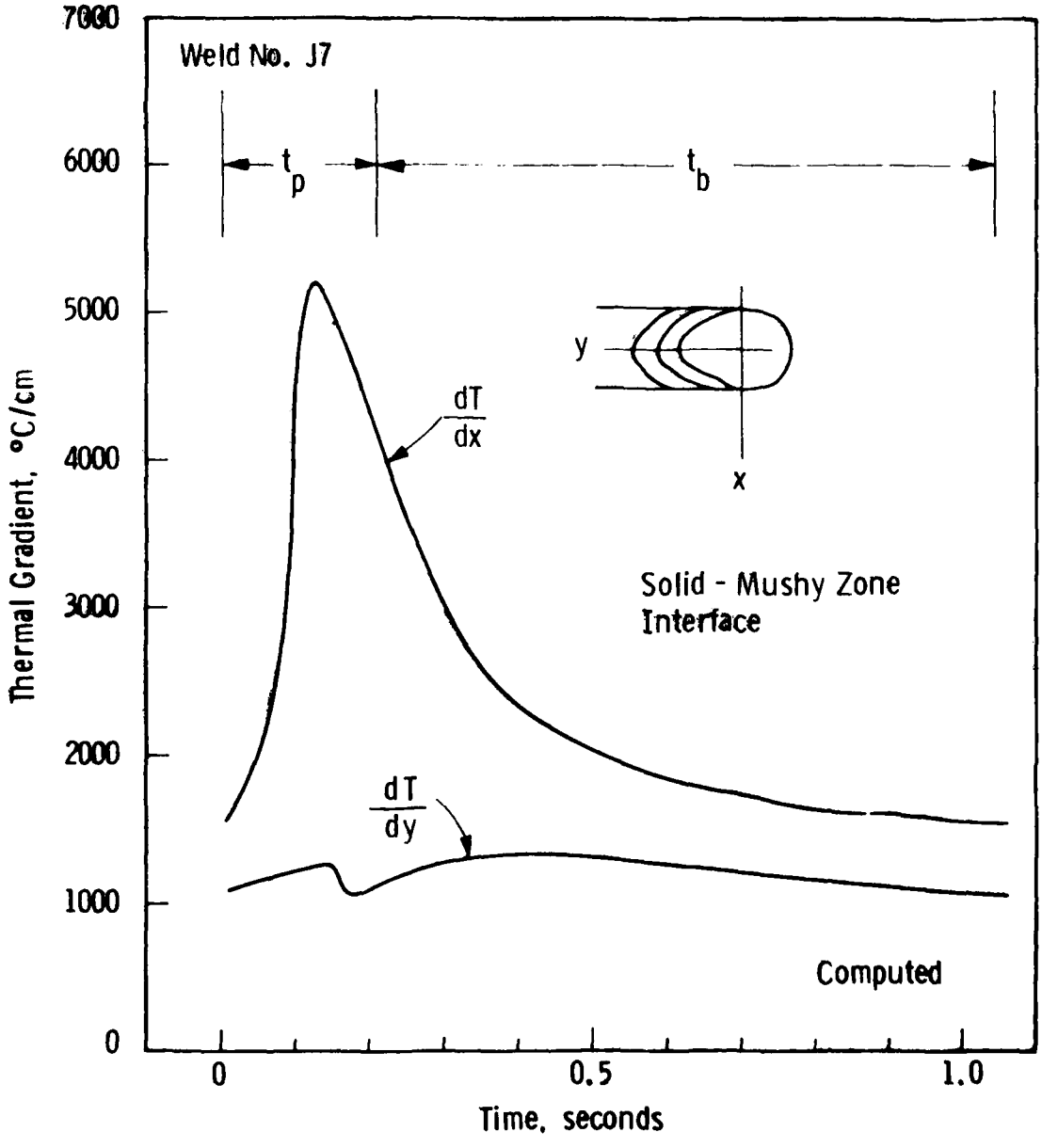

Fig. 13 – Variation of the computed thermal gradients at the solid-mushy zone interface along x and y axes (with the arc at the origin) of the weld pool

Curve 723685-A

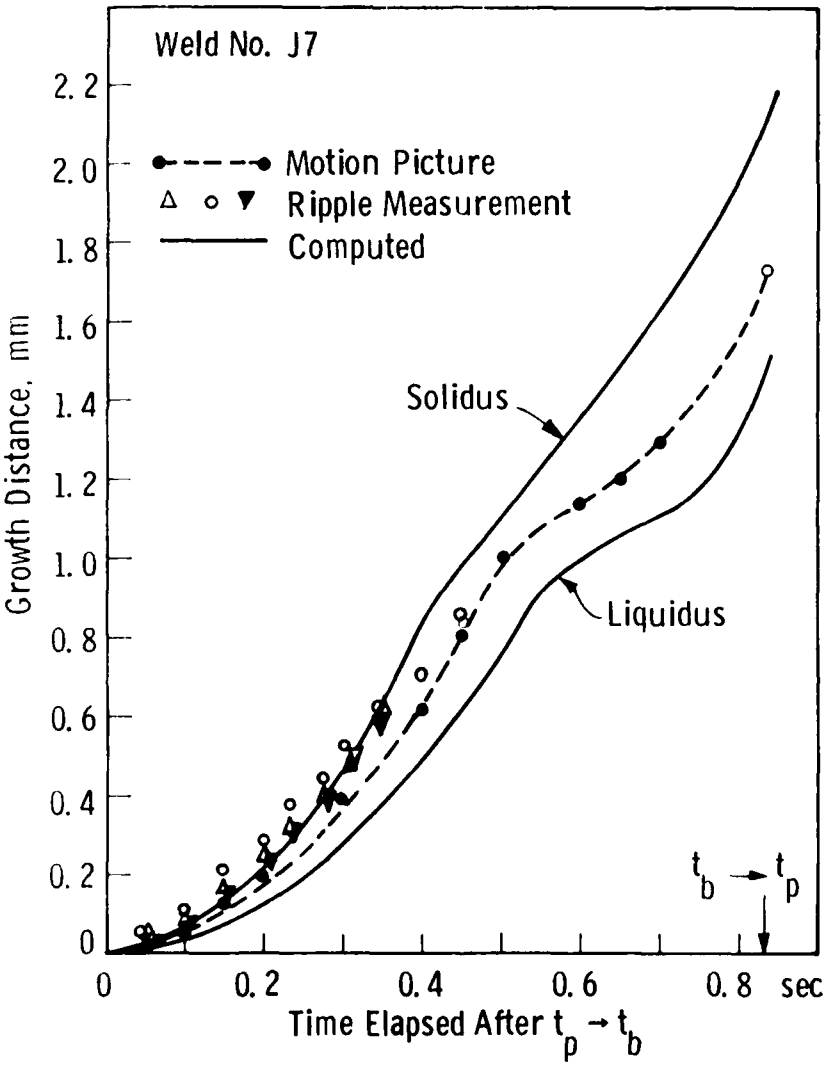

Fig. 14 — A comparison of the computed and experimentally determined movements of the solidus and the liquidus isotherms at the trailing edge of the weld pool. The data are for a single low pulse period about 14 seconds after the start of welding

PART III

GRAIN STRUCTURE AND HOT CRACKING

IN PULSED CURRENT GTAW OF AISI 321 STAINLESS STEEL

A. A. GOKHALE and H. D. BRODY

UNIVERSITY OF PITTSBURGH
PITTSBURGH, PA 15261

and

G. M. ECER

WESTINGHOUSE R&D CENTER
PITTSBURGH, PA 15235

ABSTRACT

Effects of operating parameters on the solidification structures in pulsed current gas tungsten arc welding were studied on a series of bead-on-plate welds on 0.3175 cm thick AISI 321 stainless steel. Current waveform, ratio of high and low pulse times and current frequency were found to influence the fusion zone microstructure. To study the effects of grain refinement on the properties of the weld, hot cracking tendency of stainless steel welds was estimated by using the Varestraint test. Data was reported on total number of cracks and crack lengths, in a semiquantitative fashion. Grain refinement was shown to improve the resistance of the weld bead against hot cracking.

INTRODUCTION

Since its development in the early sixties, the pulsed current gas tungsten arc welding (PC-GTAW) process has been found to have a number of advantages over the conventional, continuous current gas tungsten arc (GTA) welding process. These advantages include: arc stability, lower heat input requirements, improved tolerance to heat sink variation, better penetration control and grain refinement of the weld pool.[1-8]

Due to increased arc stability, bead contour is improved and hence precision welding is possible. Because of better penetration control, this process is well-suited to welding of thin sheets and tubes where burn-through is a common problem. Lower heat requirements reduce distortion in the plates and give rise to smaller heat affected zones (HAZ). Improved tolerance to heat sink variation makes PC-GTAW ideal for automation and for welding dissimilar metals. Through its grain-refining capabilities, PC-GTAW could be used to improve the solidification structure and the resulting properties of the weld.

In order to make proper use of the advantages offered by the PC-GTAW process, it becomes essential to know the correlations between the welding variables, the solidification structures and the resultant properties of the weld. As illustrated in Figure 1, PC-GTAW enables better control over the welding process by offering a number of independently controlled variables: peak current, i_p, background current, i_b, peak pulse duration, t_p, background pulse duration, t_b, peak to background duration ratio, t_p/t_b, travel speed, v, pitch, $v(t_p+t_b)$, and arc modulations at a variety of frequencies.

Several attempts have been made to grain refine the weld pool in various welding processes. These methods include weld pool inoculation, surface nucleation by gas impingement, arc oscillations,

etc. The methods investigated are associated with certain disadvantages such as bead embrittlement due to formation of undesirable compounds, gas entrapment, etc. A method free of such defects and which is employed in the present study, makes use of pulsed current with high frequency current modulation superimposed on the usual low-frequency square wave. It is intended that a sufficient number of heterogeneous growth sites are created by the interaction (to be discussed later) of the current pulsing and modulation with the growing solid-liquid interface to disrupt columnar growth. The grain structure modification, thus achieved, should have desirable effects on the weld properties.

The objectives of the present investigation are to grain refine the weld bead microstructure by adjusting the welding parameters and study the effects of structure modification on hot cracking of the weld.

The hot cracking properties were evaluated by Varestraint tests on sheets of AISI 321 stainless steels. The current waveforms illustrated in Figure 1, steady and pulsed current, with and without superimposition of a high frequency current modulation, were used to make the welds. Weld microstructures were studied. The number and the lengths of weld zone cracks were reported, semiquantitatively. The susceptibility to hot cracking was seen to increase with the grain size and the extent of the columnar zone.

BACKGROUND

Columnar to Equiaxed Growth Transition and Growth Substructures

Nature of transition from columnar to equiaxed growth are less common in welds compared to casting and ingot solidification. This is caused ahead of the growing solid-liquid interface due to severe thermal conditions existing in the pool. Near the surface of the pool, the thermal gradients are relatively low and, hence, conditions are more favorable for equiaxed growth.

High alloy contents are associated with more cellular/dendritic constitutional supercooling thus enabling the survival of heterogeneous growth sites available, if any. A dendritic interface can supply such growth sites if the dendrites are remelted and carried to the supercooled region ahead of the interface.[9,10] Thus, a low G/R ratio, such as exists near the weld centerline, favors equiaxed growth. It has been suggested[11] that convection might be responsible for fracturing and then carrying the dendrites ahead of the interface.

It must be mentioned also that convection in the pool, through its effects on heat and mass transfer during solidification, affects both the type and size of substructure in local areas. The available literature shows lack of systematic experimentation in this area.

Effects of Grain Structure on Solidification Cracking

The presence of intergranular liquid films during the terminal stages of solidification is at the root of solidification cracking.[12] When the thermal strains applied across adjacent grains exceed the ductility of the system, the films are ruptured without healing. Solidification cracking is favored by factors which decrease the

solid-solid contact area during the last stages of solidification. This concentrates stresses at a relatively small number of solid bridges in the weld pool. These factors include: (a) low melting point segregates and (b) large grain size. Low melting point segregates remain liquid even at lower temperatures, decreasing the solid-solid contact between the grains which are under thermal stresses. The larger the grain size, the smaller is the area of grain-boundary contact for a given liquid content. Thus, coarse-grained weld metals are more susceptible to solidification cracking.[13]

It is suggested that during weld pool solidification, the solute rich liquid from both solidification fronts tends to be trapped at the weld centerline. The concentration of low melting liquid along the centerline makes this region more prone to cracking. Tear-drop shaped pools, where angle of impingement of growth fronts is steeper, and cooling rates and thermal gradients are higher, are more susceptible to cracking than elliptical pools. In case of ferrous alloys, sulfur and phosphorus are the chief impurities which give rise to low freezing eutectics and, hence, should be kept to the lowest possible level.[13,14]

Solidification Cracking in Stainless Steel Welds

It has been observed[15] that hot cracking in austenitic stainless steel weldments is reduced or prevented when a small amount of delta ferrite is present. Hull's studies support the fact that 5-10 vol-% delta ferrite in weldments and castings afford the best resistance to hot cracking and hot tearing.[16]

Several theories on hot cracking of stainless steel weldments [illegible] been compiled by Cieslak and Savage.[17] The "shrinkage-brittleness" [illegible] associated a semi-rigid, "coherent" dendritic network which is [illegible] cracking if shrinkage strains exceed some critical [illegible] and theory of "super-solidus cracking" postulates

that a semi-continuous liquid film exists in the weldment of casting separated by bridges of solidified material. The solid-bridges, when subjected to a critical level of induced strain will fracture, forming hot cracks.

Microsegregation of impurities also plays an important role in stainless steel weld hot cracking. Elements like silicon, molybdenum, sulfur and phosphorus, which are more soluble in delta-ferrite, are rejected to the liquid during primary austenite solidification.

Sulfur and phosphorus form low melting eutectics between sulfides and phosphides and silicon tends to form glassy silicate films. These low melting compounds tend to occupy the interdendritic regions during the terminal transient period, and thus cause hot cracking.

Refinement of Structures and Its Effects on Properties

The typical columnar "as cast" structure of a weld is associated with defects such as solidification cracking, mechanical anistropy, porosity and low toughness level. It means that there is need for the control of solidifying weld pools to obtain desirable structures. The severe thermal conditions and the absence of a separate nucleation event make it difficult to apply grain refining techniques such as innoculation or dendrite fragmentation. In controlling the grain structure, it is necessary both to produce growth sites for new grains and to insure that they survive.

Surface Nucleation and Growth

Grain refining was achieved by directing an argon stream on the pool surface ahead of the arc. Evidently some of the solid formed survived the passage of the arc and acted as a source of growth sites for new grains at the advancing solidification front.[18] For complete

grain refinement, enough solid fragments had to be supplied to physically block further columnar development at all points on the advancing interface. Complete grain refinement was reported over a range of welding speeds and currents. Under these conditions, a very marked reduction in solidification crack susceptibility was recorded for an equiaxed weld bead as compared to unrefined weld beads.

Dynamic Action of the Arc (Arc Modulation)

This method of refining the weld structure consists of applying powerful short-term current pulses to the arc. The current pulses influence the solidifying pool thermally and mechanically, causing periodic shaking of the liquid metal with a frequency equal to that of the pulses. The force of the mechanical action of the arc on the metal (the arc pressure) is proportional to the square of the amplitude of the current, and the thermal energy depends on the shape and duration of the pulses, and their frequency, and on the current. The thermal effect on the liquid metal can therefore be varied within relatively wide ranges.

The application of the current pulses in case of aluminum, titanium and nickel-base alloys resulted in breaking down of the columnar structure (i.e., grain refinement). The current pulses are believed to generate fluctuations in the growth process. Such growth rate fluctuations can yield an effective supply of growth sites by the mechanism of dendrite remelting.[18,19]

The refining effect was observed only within a specific frequency range. Weld quality was shown to depend also upon the point of application of the arc. The tail part of the pool is the most suitable area, since applying current pulses near the active spot (below the arc) might cause burnthrough due to low surface tension of the metal in this region. Also, the tail part being away from the arc, is cooler as compared to the rest of the pool; this makes survival of growth sites

easy. Use of an additional arc near the trailing edge of the pool can thus help refine the grain structure. The dynamic action of the arc increases the dispersion of oxide film inclusions, present if any, in the weld metal.

The grain refined welds are shown to improve their hot cracking resistance and other mechanical properties. Davies and Garland report that pulsing of the arc alone does not seem to generate effective grain or substructure refinement.[13] They have deomstrated for AISI 321 stainless steel that if current modulation is superimposed on the pulse, significant effects can result.

Weld Pool Innoculation

Garland has reported some success in achieving grain refinement in Al/1.7-2.8% Mg weld pools by innoculating them with Fe-Ti powder. The mechanism of this refinement was based on the formation of heterogeneous nuclei in the pool. Rate of innoculant supply, position of innoculation in the pool, size of the innoculant powder and welding conditions affect the grain refining ability of the innoculants. Embrittlement could be caused due to the formation of undesirable compounds by chemical reaction of innoculant with the metal.[20]

Electrode Vibration

Mechanical vibration of the electrode is also reported to have beneficial effects on structure of the weld. But the physical disturbance caused in the pool is often not sufficient to achieve complete grain refinement.

To summarize, the effects of grain refinement techniques include improved weld metal properties and fewer defects. Reduction in solidification cracking has been reported.

EXPERIMENTS

As mentioned earlier, the present investigation was aimed at analysing the grain refining effects of pulsed current and related waveforms, and to see the effect of grain refining on the hot cracking tendency of stainless steel welds. The Varestraint test was used to evaluate the susceptibility to hot cracking of welds made under a variety of waveforms. (See Figure 1.) Metallographic specimens were then cut out of the Varestraint test specimens and studied under the optical microscope to see if any grain refinement had taken place.

Varestraint Testing

The cracking test used in the present investigation, the Subsize Varestraint Test, employs 1 in. x 6 in. x 1/8 in. (2.5 x 15 x 0.3 cm) specimens. The standard equipment used is shown schematically in Figure 2. Welding starts at one end of the plate. As the electrode moves past a particular location, a sudden force is applied pneumatically at the end of the plate where welding was initiated. Due to this force, and because the plate is clamped at the other end, it bends till it conforms to the curved surface of the die block. Due to this bending, a certain amount of strain is given to the plate which makes the weld crack while it is solidifying. The amount of strain can be controlled by using a suitable curvature for the die block. Cracks thus formed can be studied once welding is complete and the plate has cooled down to room temperature.

The welding electrode was made of tungsten with 2% thoria. It was 1/8 in. (0.32 cm) diameter with 60° included angle and 1/32 in. (0.08 cm) diameter flat tip. Arc gap was maintained at 1/16 in. (0.16 cm). Shielding gas was pure helium flowing at a rate of 50 cfh.

Electrode velocity was maintained constant at 15 ipm (6.35 mm/sec).

The nominal composition of the stainless steel sheets used is given in Table 1. Other welding parameters are presented in Tables 2 to 5. The variables which were changed systematically were: current wave form, t_p/t_b ratio and frequency of current. Other variables were changed only moderately so as to make beads of comparable size.

Crack Analysis

Each specimen after welding and bending as described earlier, was studied under a toolmakers microscope at 20 X magnification. The area of the weld bead which underwent cracking was located and studied. A semiquantitative approach was adopted while studying cracking tendency. Specimens were grouped according to the number of cracks they formed and characterized by a "crack severity index" and characterized as well by an estimated "crack length index" (qualitative judgment). Table 6 explains the rough scale used for crack measurements. This simplified crack analysis gives a meaningful idea about the hot cracking susceptibility of the alloy under consideration.

In order to compare this semiquantitative scale of crack measurements with the "standard" scale which measures total crack length (as used in original Varestraint testing), 30-40% of the specimens which showed different degrees of hot cracking were chosen for measurement of total crack length. The normal measurement of total crack length was reported for these specimens and plotted against the crack severity index, note Figure 3. The correspondence between the measurement of total crack length and crack severity index is good. We have used the crack severity index and the average crack length indices in this study (a) because the semiquantitave measurements are less time

consuming and (b) because more information on crack behavior is retained for comparison with microstructural and welding variables.

Metallography

Metallographic specimens were cut from the welded plates, polished and etched with an acid mixture (30 water:20 HCl: HNO3). Figure 4 explains three different sections polished and etched. This etch revealed the substructure boundaries. Different regions were characterized as having either a columnar or equiaxed grain structure depending upon the length to width ratio of the grains. Grains with length to width ratio exceeding 2 were considered columnar. Grain boundaries were not seen clearly; hence, the cellular or dendritic substructure was used to make these estimates. The cell boundaries were identified due to the residual impurities and also in some cases, due to segregated ferrite.

Grain size was also estimated in a semiquantitative fashion and labelled as 1, 2 or 3. These notations are explained in Table 7. The structures thus studied were compared with the cracking tendencies of the welds.

RESULTS

Crack Analysis

The crack severity indices and their lengths are reported in Table 8. Only weld metal cracks formed at the instantaneous location of the solid-liquid interface at the time of bending, were taken into consideration. Cracks were almost invariably initiated at the solid-liquid interface and they propogated in a direction perpendicular to the interface. Cracks formed near the weld centerline were usually found to be longer than others.

Microstructures

As shown earlier by other investigators, initial growth seemed to be epitaxial in nature.[13,14] Grain structure in the heat affected zones (HAZ) continued through the fusion line into the fusion zone over a short distance, without much change in the orientation. This is shown in Figure 5.

Grains were predominantly columnar near the fusion line, later becoming equiaxed toward the weld centerline. The relative amounts of columnar and equiaxed zones are recorded in Table 8. Figures 6 to 8 are microstructures showing varying extent of columnarity. Semiquantitative estimates were made on grain size in both columnar and equiaxed zones. Effects of structural parameters like percent columnarity and grain size on hot cracking are presented in Figures 9 to 11. In some cases where the pitch was high, successive pulses seemed to have a grain refining effect on the previously solidified beads. Portions of HAZ very close to the fusion line had undergone grain growth.

Columnarity as seen at the top surface of the bead is different from that seen either at the transverse or the longitudinal cross section of the weld. Figures 8, 12, and 13 are three different sections of the same weld specimen, showing different extents to which the structures are columnar. This is because a columnar grain if observed from a plane perpendicular to its direction of growth will appear equiaxed, while if observed from a plane parallel to its growth direction will appear truly columnar. Thus precaution must be taken while assigning a percent columnarity value to any microstructure. Table 9 gives columnarity estimates at the weld transverse cross section. In the present case, however, it is found that the region near the weld surface is truly equiaxed as it appears so in all three mutually orthogonal planes.

DISCUSSION

Weld Bead Grain Structures

As reported in the results, growth is epitaxial in most cases, i.e. the grain structure in the base metal seems to continue through the fusion line into the fusion zone. Solidification takes place in the absence of a separate nucleation step. Also, no new grain boundaries have to be created to start the growth. Both these factors reduce the activation energy of the phase transformation, thus making epitaxial growth energetically favorable.

The initial epitaxial growth is followed by the process of competetive growth. Grains with a preferred crystallographic direction most nearly parallel to the directions of the maximum thermal gradient, grow at the expense of other less favorably oriented grains. This gives rise to a zone of columnar grains. This columnar zone may or may not extend up to the weld centerline depending upon the welding conditions. For example, the columnar zone occupies 80-90% of the bead area (as seen in the top view) in specimens 1-8 and 1-6; about 50% in specimens 2-6 and 2-7, and 0-10% in specimens 2-9, 2-2 and 4-1. The region near the weld centerline normally consists of equiaxed grains. One of the reasons behind the formation of the equiaxed grains is the creation of heterogeneous growth sites in the solidifying puddle. When the current pulse is superimposed with a high frequency modulated current, the growing solid-liquid interface is subjected to thermal disturbances causing remelting of the dendrites.

This is further enhanced by a mechanical action of the pool turbulence in bringing the dendrites ahead of the solid-liquid interface. These dendrites then become sites for heterogeneous growth which eventually blocks the columnar growth process. Repeated

interruption of the columnar growth gives rise to a zone of equiaxed grains.

In the case of pulsed current welds each pulse seems to have a grain refining effect on the bead deposited by the previous pulse. A distinct zone is seen near the fusion line which seems to have gone through a heating cycle due to the following pulses (Figures 6-8). Each bead, after solidification is subjected to heating and cooling caused by successive current pulses. The bead passed through the critical temperature range of the material every time refining the grain structure. Here the "critical temperature" refers to the solid-state transformation temperature, as shown in Figure 14. The type of waveform seems to have some effect on the grain structure of the weld. Pulsation of the current alone causes considerable turbulence in the pool. But even with a pulsating current, in many cases, liquid in the region next to the trailing interface appeared stagnant in the movies. The stagnant layer could possibly be disturbed by superimposing the high frequency modulation, thereby carrying the mechanical and thermal disturbances given by the arc to the interface more effectively.

Arc modulation does seem to have a beneficial effect on the grain structure when coupled with a low t_p/t_b ratio and high pitch. The latter two conditions produce cooler weld pools, thereby making it easier for heterogeneous growth sites to survive.

Hot Cracking

Figures 9 to 11 show that grain structure in the weld bead has a considerable influence on the amount of cracking taking place during Varestraint tests. It is observed that the cracking severity increases with increase in the percentage columnarity and

the grain size. These results could be partially explained with the help of the generalized theory of "super-solidus cracking" (discussed earlier). When the primary phase to solidify is austenite, elements such as silicon, sulfur and phosphorus, which are more soluble in delta ferrite, are rejected to the liquid. Sulfur and phosphorus form low melting eutectics between sulfides and phosphides. Due to the presence of these liquid compounds at high temperatures, the grain boundaries become considerably weaker, and hence, a lateral stress (such as thermal stress due to uneven expansion and contraction in welding) existing at such high temperatures can easily pull apart adjacent grains along the boundary between them. Also, the presence of the liquid film reduces the solid-solid contact area between the grains thereby increasing the stress concentration level. A moderate amount of delta ferrite (about 4-7%) is reported to reduce hot cracking, by dissolving the harmful impurities like sulfur and phosphorus. This may be one of the reasons for the relatively low severity of cracking found in 321 welds.

When a structure is columnar, the eutectic films are more continuous thus leaving very small solid-solid contact area. This results in a higher degree of cracking severity. Also, a crack once initiated, can propogate along the columnar grain boundaries easily without having to change its direction. The grain refinement was observed to be restricted near the weld surface. The cracks, also, were seen to be very thin, mostly confined to the surface region, where the Varestraint test strain was maximum. Thus the above explanation still holds good in the present case.

A coarse grain structure has a low grain surface area per unit volume. Thus, for a given amount of eutectic, it spreads over a smaller grain boundary area thereby increasing their concentration. This

weakens the grain boundaries even further thus making the structure more susceptible to cracking.

Centerline cracks were usually found to be larger than the cracks formed near the fusion line. Centerline segregation may be one of thc reasons behind this phenomenon. Beads having a circular cross section were found to be more susceptible to hot cracking than flat beads. The exact explanation for this observation does not exist but studies on the effects of bead shape on the grain orientation and on the thermal stresses may throw some light in this area.

No single welding variable seems to affect hot cracking. But a combination of the waveform, t_p/t_b ratio and the pitch could reduce the crack severity. In the present investigation, superimposing high frequency current modulation on a pulsed current, having low t_p/t_b ratio (0.1-0.2) and high pitch (2-3 mm) is believed to reduce the hot cracking susceptibility of AISI 321 stainless steel welds.

CONCLUSIONS

(1) Grain structure in the bead can be refined by adjusting the operating (welding) parameters.

(2) Low t_p/t_b ratio (0.1-0.2), high pitch (2-3 mm), and arc modulation seem to be beneficial in grain refining weld bead microstructure.

(3) Weld bead microstructure influences hot cracking susceptibility in AISI 321 stainless steel. The occurrence of hot cracking is reduced by having a predominantly equiaxed structure and having a fine grain size.

ACKNOWLEDGEMENTS

This research was sponsored by the Office of Naval Research, Contract N00014-77-C-0596, Dr. Bruce MacDonald, Scientific Officer. The authors are grateful to Dr. Alexander Tzavaras, Aristotelean University, Salonica, Greece for helpful discussions and Ms. Jeri Frizza and Mr. John Farinelli of the University of Pittsburgh and Mr. Richard Berrier of Westinghouse R&D Center for help with the experimental phases of this work.

AD-A097 392 WESTINGHOUSE RESEARCH AND DEVELOPMENT CENTER PITTSBU--ETC F/G 13/8
INVESTIGATION OF WELD POOL STRUCTURE AND PROPERTY CONTROL IN PU--ETC(U)
MAR 80 G M ECER, G G LESSMANN, H D BRODY N00014-77-C-0596
UNCLASSIFIED 81-9D4-PULSE-R1 NL

REFERENCES

1. Trofimov, N. M., "Stability of DC Arc Burning in Welding With A Non-Consumable Electrode," Welding Production, Vol. 20, No. 8 (August 1975), pp. 6-11.

2. Dudko, D. A., et al., "Improving the Stability of the Low-Amperage Argon-Shielded Arc," Automatic Welding, Vol. 28, No. 11 (November 1975), pp. 10-11.

3. Boughton, P. and Males, B. O., "Penetration Characteristics of Pulsed TIG-Welding," Pulsed TIG-Welding Seminar Handbook, The Welding Institute, Abington, England (1973).

4. Stoeckinger, G. R., "Pulsed DC High Frequency GTA Welding of Aluminum Plate," Welding Journal, Vol. 52 (1973), pp. 558-s-567-s.

5. Vilkas, E. P., "Pulsed Current and Its Applications," Welding Journal, Vol. 49 (1973), pp. 255-262.

6. Needham, J. C., "Pulsed Current Tungsten Arc Welding," Pulsed TIG-Welding Seminar Handbook, The Welding Institute, Abington, England (1973).

7. Boughton, P., "High Precision Pulsed TIG-Welding," Pulsed TIG Welding Seminar Handbook, The Welding Institute, Abington, England (1973).

8. Garland, J. G. and Davies, G. J., "Surface Rippling and Growth Perturbations During Weld Pool Solidification," British Welding Journal, Vol. 18 (1970), pp. 171-175.

9. Jackson, K. A., Hunt, J. D., Uhlmann, D. R., and Seward, T. P., III, "On the Origin of the Equiaxed Zone in Castings," Transactions of the Metallurgical Society of AIME, Vol. 236 (1966), pp. 149-158.

10. Uhlmann, D. R., Seward, T. P., III, and Chalmers, B., "The Effects of Magnetic Fields on the Structure of Metal Alloy Castings," Transactions of the Metallurgical Society of AIME, Vol. 236 (1966), pp. 527-531.

11. Flemings, M. C., Solidification Processing, McGraw-Hill, New York (1973), pp. 154-157.

12. Pellini, W. S., "Strain Theory of Hot Tearing," Foundry, November 1952, pp. 125-133, 192-199.

13. Davies, G. J. and Garland, J. G., "Solidification Structures and Properties of Fusion Welds," International Metallurgical Reviews, Vol. 20 (1975), pp. 83-106.

14. Savage, W. F. and Aronson, A. H., "Preferred Orientation in Weld Fusion Zone," Welding Journal, Vol. 45 (1966), pp. 85-s-89-s.

15. DeLong, W. T., "Ferrite in Austenitic Stainless Steel Weld Metal," Welding Journal, 35(11), November 1956, Research Suppl. pp. 273-s-286-s.

16. Hull, F. C., "Effect of Delta Ferrite on the Hot Cracking of Stainless Steel," Welding Journal, Vol. 46 (1967), pp. 399-2-409-s.

17. Cieslak, M. J. and Savage, W. F., "Weldability and Solidification Phenomena of Cast Stainless Steel," Welding Journal, Vol. 59 (1980), pp. 136-s-146-s.

18. Slavin, G. A., Masalova, N. D. and Morozova, T. V., "The Relationship Between Technical Strength and Solidification in the Pulsed-Arc Welding of Creep-Resisting Alloys With Non-consumable Electrodes," Welding Production, Vol. 18, No. 6 (June 1971), pp. 26-29.

19. Slavin, G. A., et al., "Control of the Solidification Process by Means of a Dynamic Action of the Arc," Welding Production, Vol. 21, No. 8 (August 1974), pp. 3-4.

20. Garland, J. G., "Weld Pool Solidification Control," British Welding Journal, Vol. 22 (1974), pp. 121-127.

TABLE 1

NOMINAL COMPOSITION OF 321 STAINLESS STEEL PLATES

C	Mn	Cr	Ni	Ti	Fe
0.08 Max.	2.0	17 - 19	9 - 12	5x%C Min.	Balance

TABLE 2

OPERATING PARAMETERS FOR 321 STAINLESS STEEL WELDING

Waveform 1: Steady Current

Specimen No.	Average Current I amp.	Varestraint Test Strain %
1-1	60	2
1-2	60	2
1-3	60	3
1-4	60	4
1-5	70	4
1-6	70	4
1-7	65	4
1-8	60	4
1-9	60	4
1-10	55	4

TABLE 3

OPERATING PARAMETERS FOR 321 STAINLESS STEEL WELDING

Waveform 2: Low Frequency Pulsed Current
(All Varestraint Test Strains at 4%)

Specimen No.	i_p amp.	i_b amp.	t_p sec	t_b sec	Average Current I amp.
2-1	130	10	0.060	0.108	52.8
2-2	130	10	0.060	0.108	52.8
2-3	130	10	0.030	0.054	52.8
2-4	130	10	0.030	0.054	52.8
2-5	130	10	0.006	0.022	51.8
2-6	130	10	0.005	0.011	52.3
2-7	130	10	0.005	0.009	52.8
2-8	130	10	0.120	0.009	52.8
2-9	130	10	0.060	0.216	52.8
2-10	150	20	0.060	0.135	60.0
2-11	150	30	0.060	0.180	60.0
2-12	150	40	0.060	0.270	60.0
2-13	150	50	0.060	0.540	60.0
2-14	150	50	0.060	0.540	60.0
2-15	150	50	0.060	0.540	60.0
2-16	130	42	0.060	0.360	55.0
2-17	130	42	0.060	0.360	55.0

TABLE 4

OPERATING PARAMETERS FOR 321 STAINLESS STEEL WELDING

Waveform 3: Steady Current + HF Modulation
(All Varestraint Test Strains at 4%)

Specimen No.	Average Current I amp.	Modulation Frequency KH_z	Modulation Amplitude I_m amp.
3-1	60	2	50
3-2	60	6	50
3-2	60	8	50
3-4	60	2	50
3-5	60	4	50
3-6	60	4	50
3-7	60	6	50
3-8	60	8	50

TABLE 5

OPERATING PARAMETERS FOR 321 STAINLESS STEEL WELDING

Waveform 4: Low Frequency Pulsed Current + High Frequency Modulation
(All Varestraint Test Strains at 4%)

Specimen No.	i_p amp.	i_b amp.	t_p sec	t_b sec	Average I amp.	Modulation Frequency KH_z	Modulation Amplitude I_m amp.
4-1	120	25	0.120	0.216	58.9	2	20
4-2	120	25	0.120	0.216	58.9	6	20
4-3	120	25	0.120	0.216	58.9	8	20
4-4	130	42	0.060	0.360	55	2	20
4-5	130	42	0.060	0.360	55	2	20
4-6	130	42	0.060	0.360	55	6	20
4-7	130	42	0.060	0.360	55	6	20
4-8	130	42	0.060	0.360	55	8	20

TABLE 6

SEMIQUANTIIATIVE SCALE FOR CRACK MEASUREMENT

Crack Severity Index (CSI)	Number of Cracks
1	0
2	1-2
3	3-6
4	7-10
5	> 10

Crack Length Index (CLI)	Range for Crack Length (mils)
S	2-4
M	5-7
L	8 and above

TABLE 7

SEMIQUANTITATIVE SCALE FOR GRAIN SIZE MEASUREMENTS

(A) Equiaxed Grains

Grain Size Index (GSI)	Range of Grain Size (microns)
1	40-45
2	60-65
3	70-75

(B) Columnar Grains (Length)

Grain Length Index (GLI)	Range of Grain Lengths (microns)
1	100-125
2	200-225
3	400-475

(C) Columnar Grains (Width)

Grain Width Index (GWI)	Range of Grain Widths (microns)
1	25-30
2	40-45
3	55-60

TABLE 8

RESULTS OF CRACK AND GRAIN STRUCTURE MEASUREMENTS

Waveform 1

Specimen No.	CSI	CLI	Columnarity %	Equiaxed	Columnar	
				GSI	GLI	GWI
1-1	3	M	60	2	2	3
1-2	2	L	30	2	2	2
1-3	1	---	30	2	1	1
1-4	5	S	60	2	3	2
1-5	5	M	60	3	3	3
1-6	3	M	90	1	3	1
1-7	4	L	60	3	2	2
1-8	5	S	80	3	3	2
1-9	5	S	50	1	2	2
1-10	2	M	80	3	2	2

Waveform 2

Specimen No.	CSI	CLI	Columnarity %	Equiaxed	Columnar	
				GSI	GLI	GWI
2-1	2	M	30	1	1	2
2-2	2	S	10	5	---	---
2-3	1	---	20	3	1	1
2-4	1	---	20	3	1	1
2-5	5	M	70	2	2	2
2-6	1	---	50	2	1	1
2-7	2	S	50	2	3	2
2-8	2	S	50	1	2	2
2-9	1	---	0	5	---	---
2-10	2	M	20	1	1	2
2-11	2	S	20	3	1	1
2-12	5	L	70	2	2	2
2-13	3	M	70	1	3	2
2-14	2	M	70	3	3	3
2-15	3	M	70	1	3	2
2-16	3	S	10	2	1	2
2-17	2	M	30	1	1	2

TABLE 8 (continued)

Waveform 3

Specimen No.	CSI	CLI	Columnarity %	Equiaxed	Columnar	
				GSI	GLI	GWI
3-1	3	M	70	2	3	2
3-2	2	S	60	2	3	2
3-3	3	M	50	2	2	2
3-4	5	L	--	---	---	---
3-5	4	S	--	---	---	---
3-6	3	M	60	3	2	2
3-7	5	M	80	3	2	2
3-8	5	S	30	2	1	2

Waveform 4

Specimen No.	CSI	CLI	Columnarity %	Equiaxed	Columnar	
				GSI	GLI	GWI
4-1	4	S	0	5	---	---
4-2	3	S	40	2	2	2
4-3	3	L	40	3	2	3
4-4	1	---	30	2	2	2
4-5	3	M	40	3	2	1
4-6	1	---	10	2	2	2
4-7	2	M	20	2	2	2
4-8	1	---	20	2	2	2

TABLE 9

ESTIMATES ON % COLUMNARITY (AISI 321 S.S.)

Specimen Number	% Columnarity (Top Section)	% Columnarity (Transverse Section)
4-1	0	60
2-9	0	55
2-2	10	25
2-4	20	15
2-10	20	35
2-3	20	20
2-11	20	20
4-3	40	40
2-8	50	20
2-7	50	15
1-4	60	15
1-8	70	30

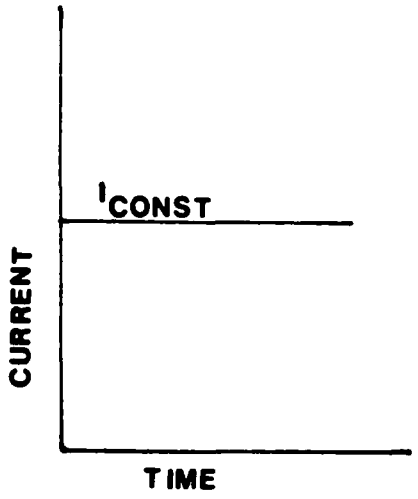

(a) Waveform 1
Steady Current

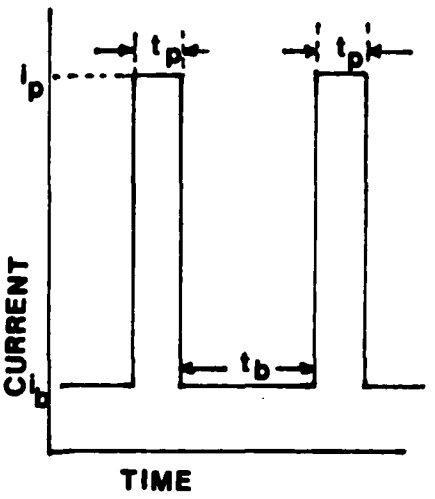

(b) Waveform 2
Pulsed Current
Low frequency (10-100 H_z)

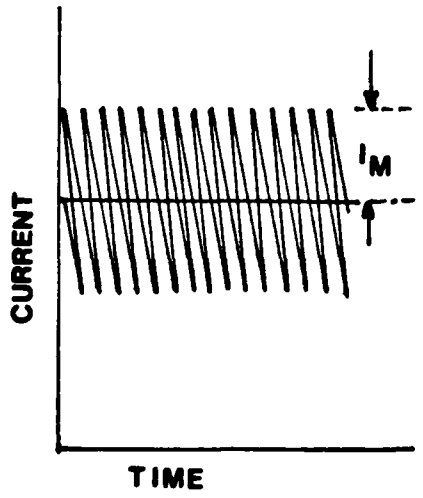

(c) Waveform 3
Steady Current + HF modulation

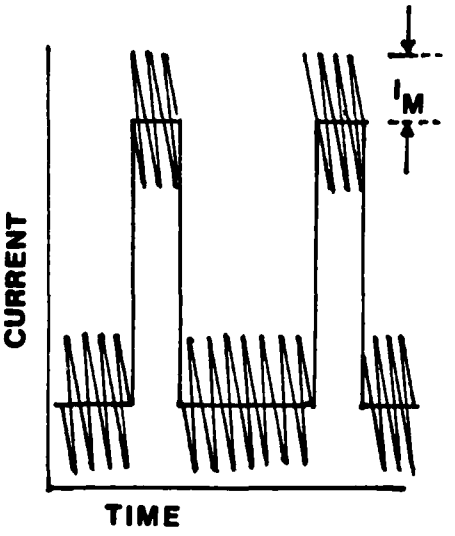

(d) Waveform 4
Pulsed Current + HF modulation

Figure 1: Current waveforms used for stainless steel welding

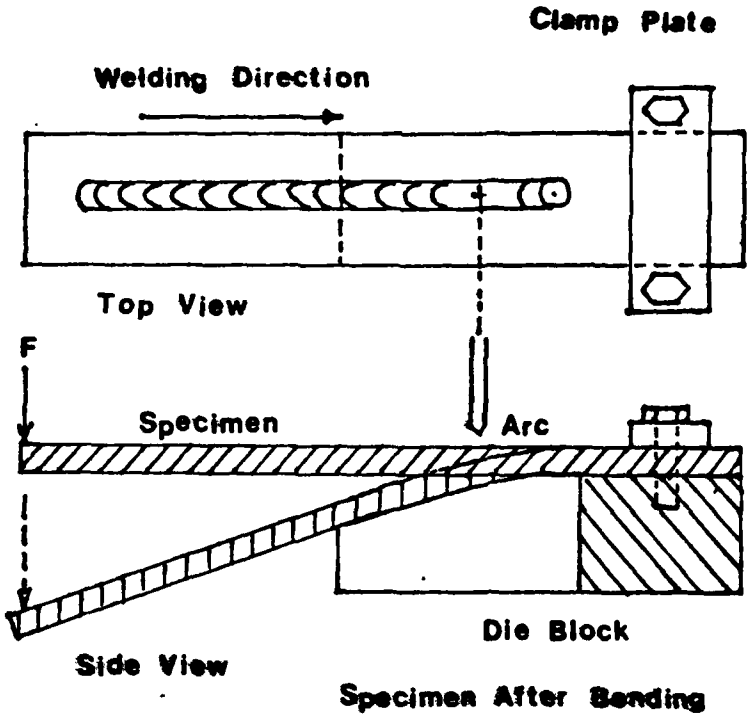

Figure 2: Subsize Varestraint test equipment (schematic)

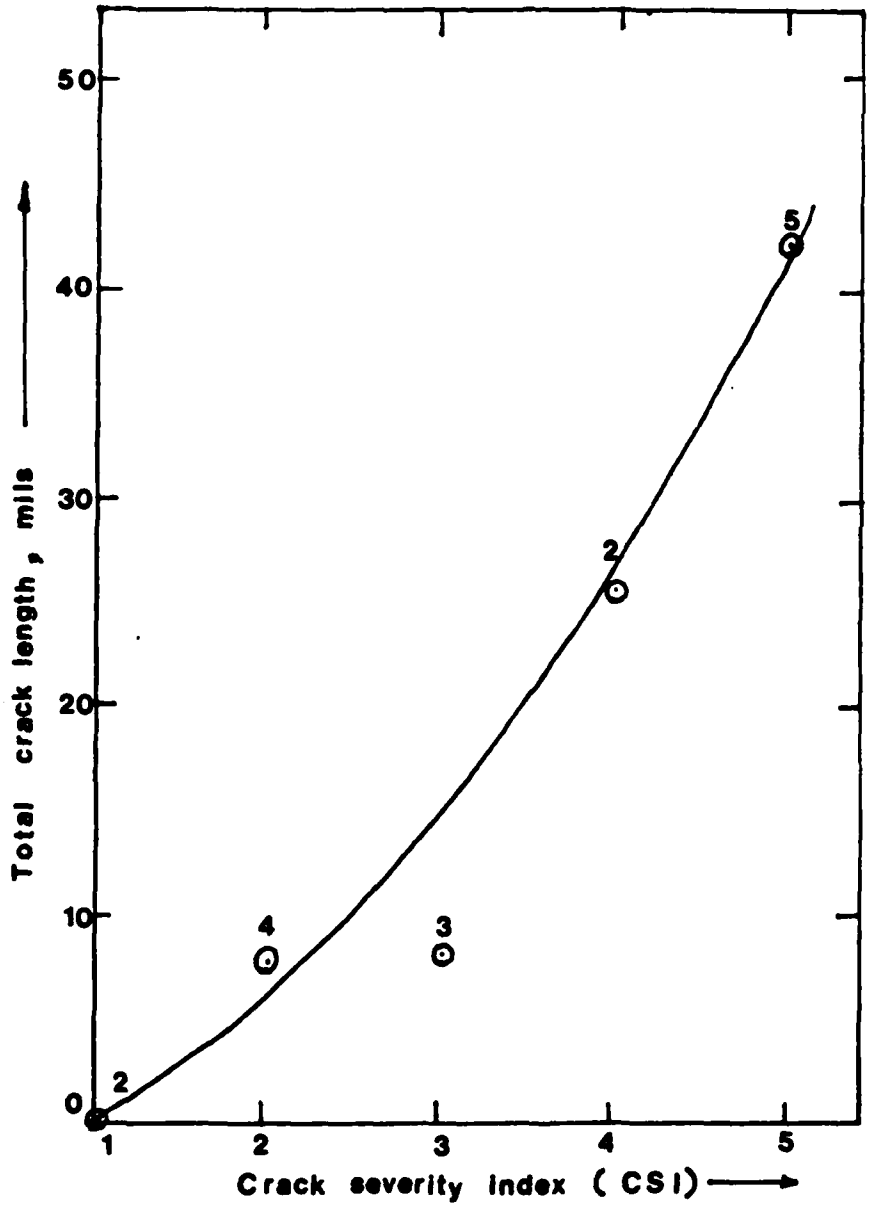

Figure 3: Comparison between the semiquantitative CSI scale and the total crack length. Number of specimens considered is shown above points on the graph.

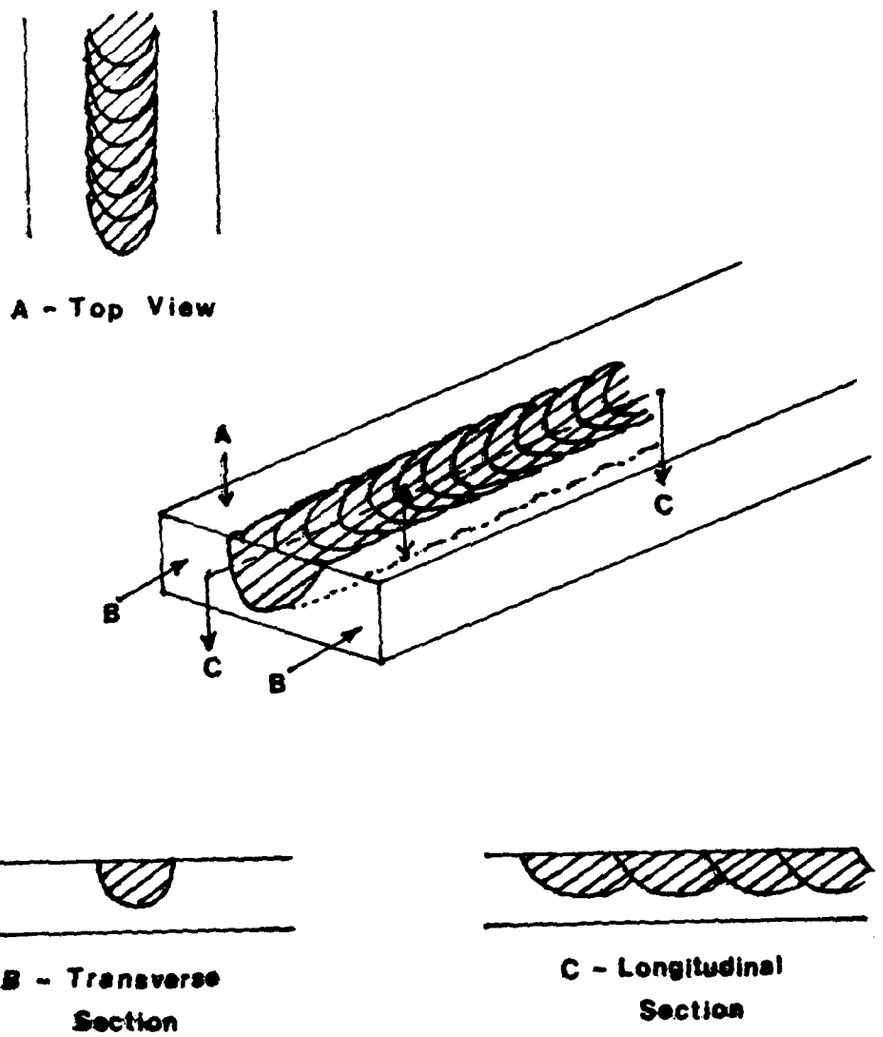

Figure 4: Sections for metallographic studies. Weld zone is shown as shaded regions.

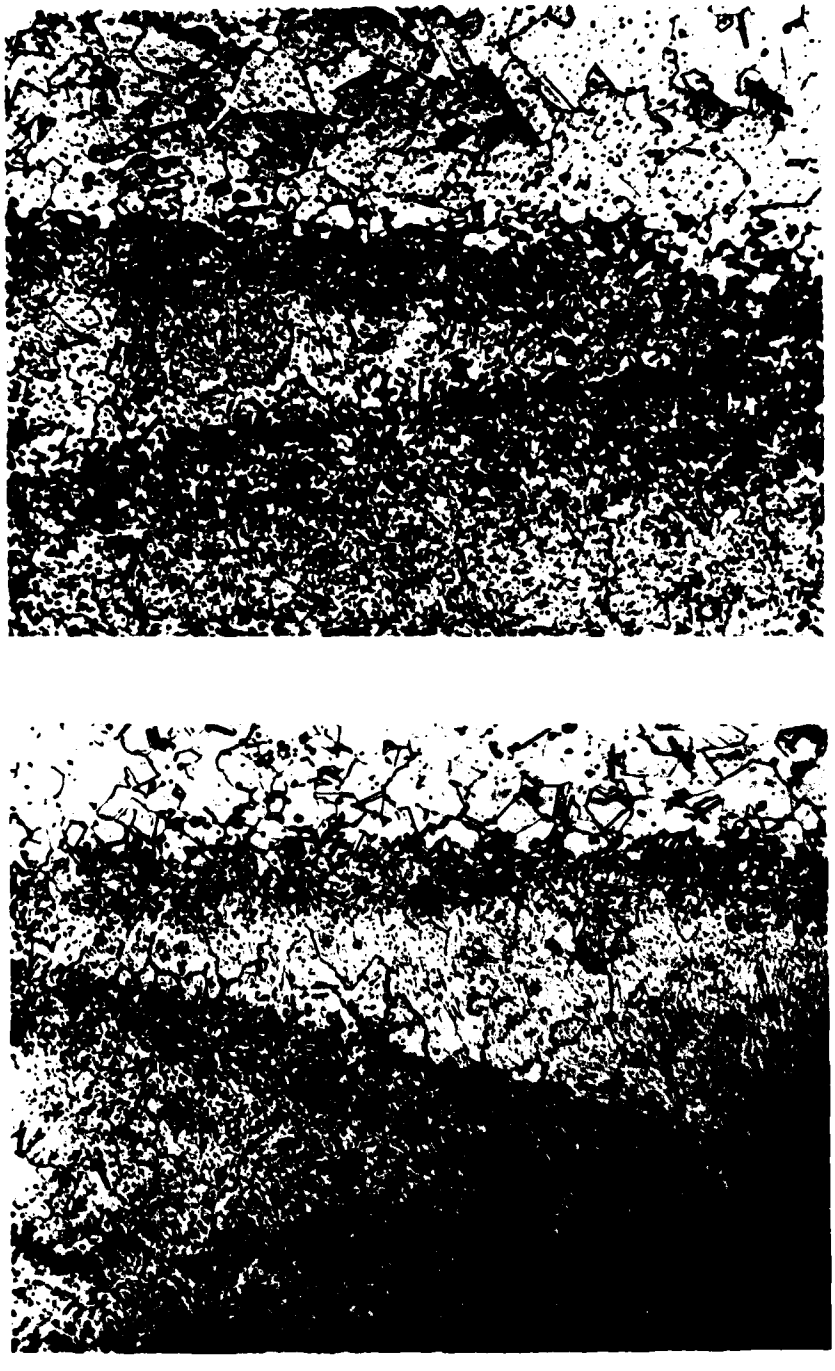

Figure 5: (a) Microstructure of the weld zone in Sepcimen No. 2-10 (top section), near thc fusion line. (b) Same view for Specimen No. 2-1. Note the similarity between structures in both sides of the fusion line. Also note the finer structure at the ripples.

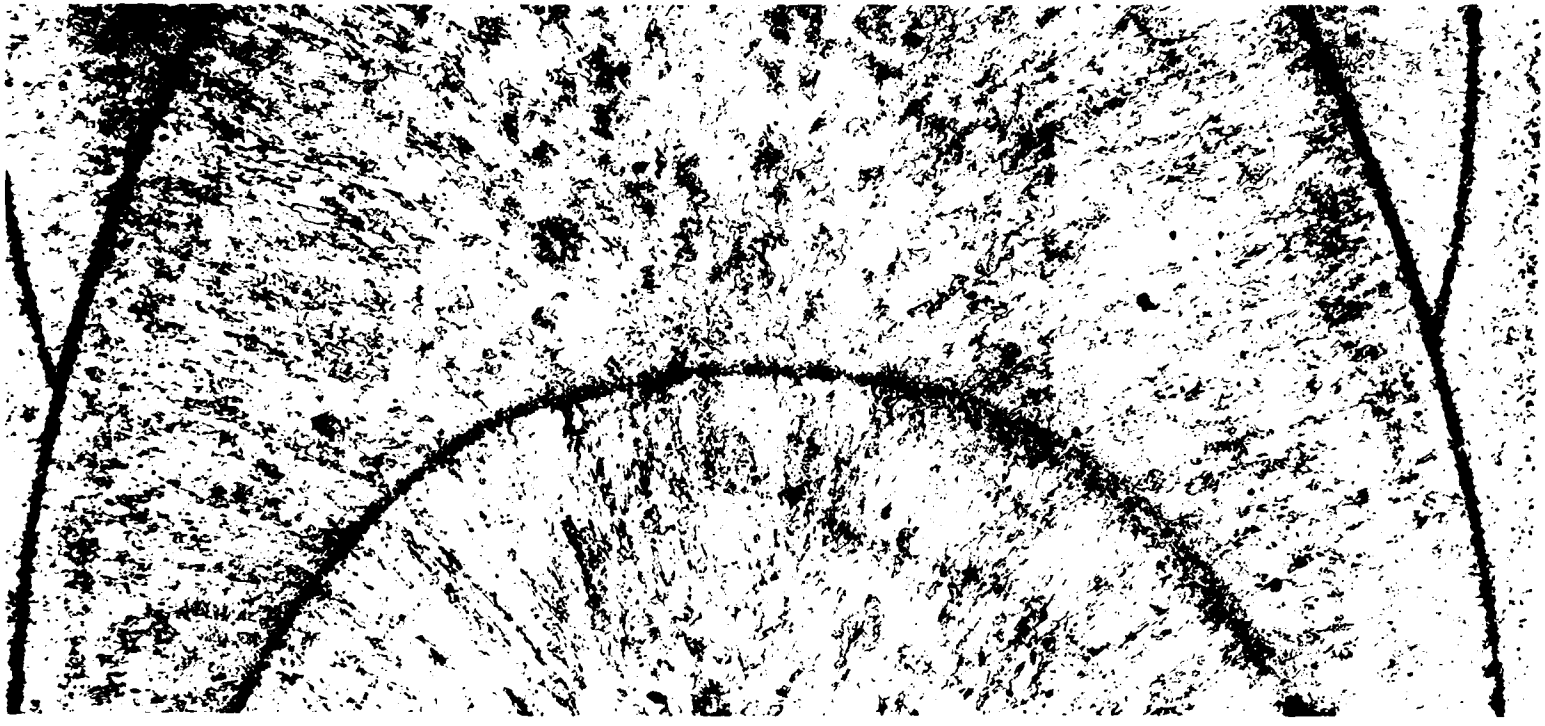

Figure 6: Microstructure of the weld zone in Specimen No. 4-2 (top section) made under waveform 4, t_p/t_b= 0.55. Estimated surface columnarity = 40%.

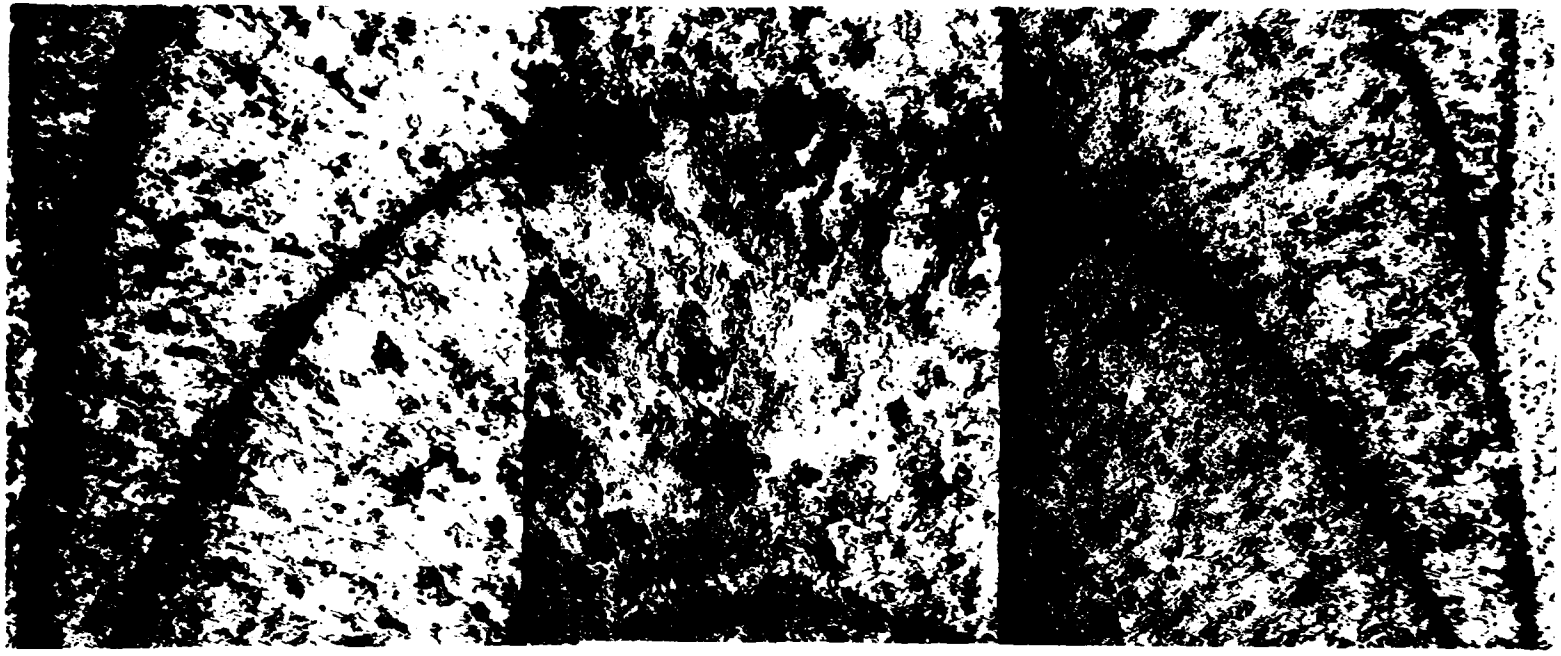

Figure 7: Microstructure of the weld zone in Specimen 2-12 (top section), made under waveform 2, t_p/t_b = 0.33. Estimated surface columnarity = 20%.

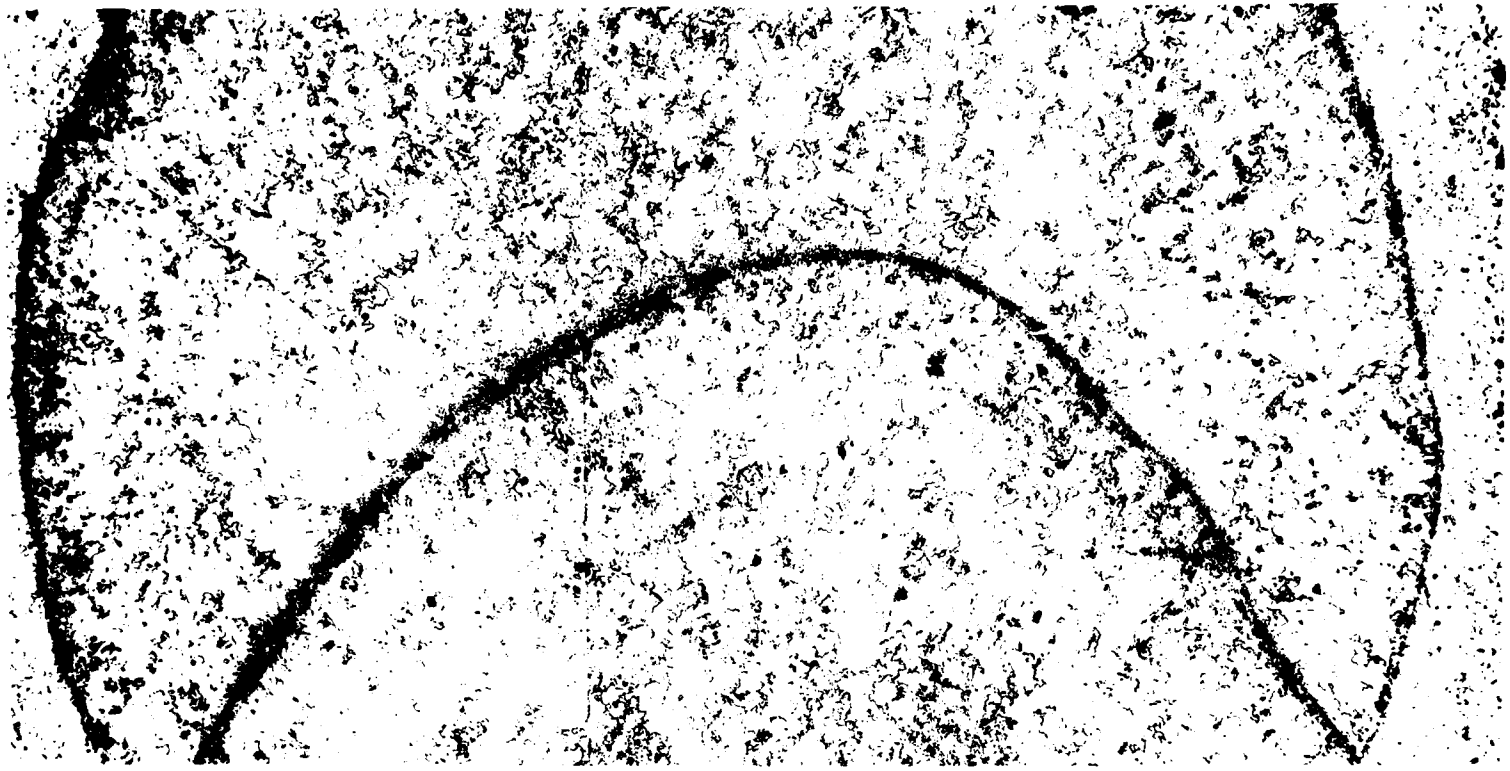

Figure 8: Microstructure of the weld zone in Specimen No. 2-9 (top section), made under waveform 2, $t_p/t_b = 0.55$. Estimated surface columnarity = 0%.

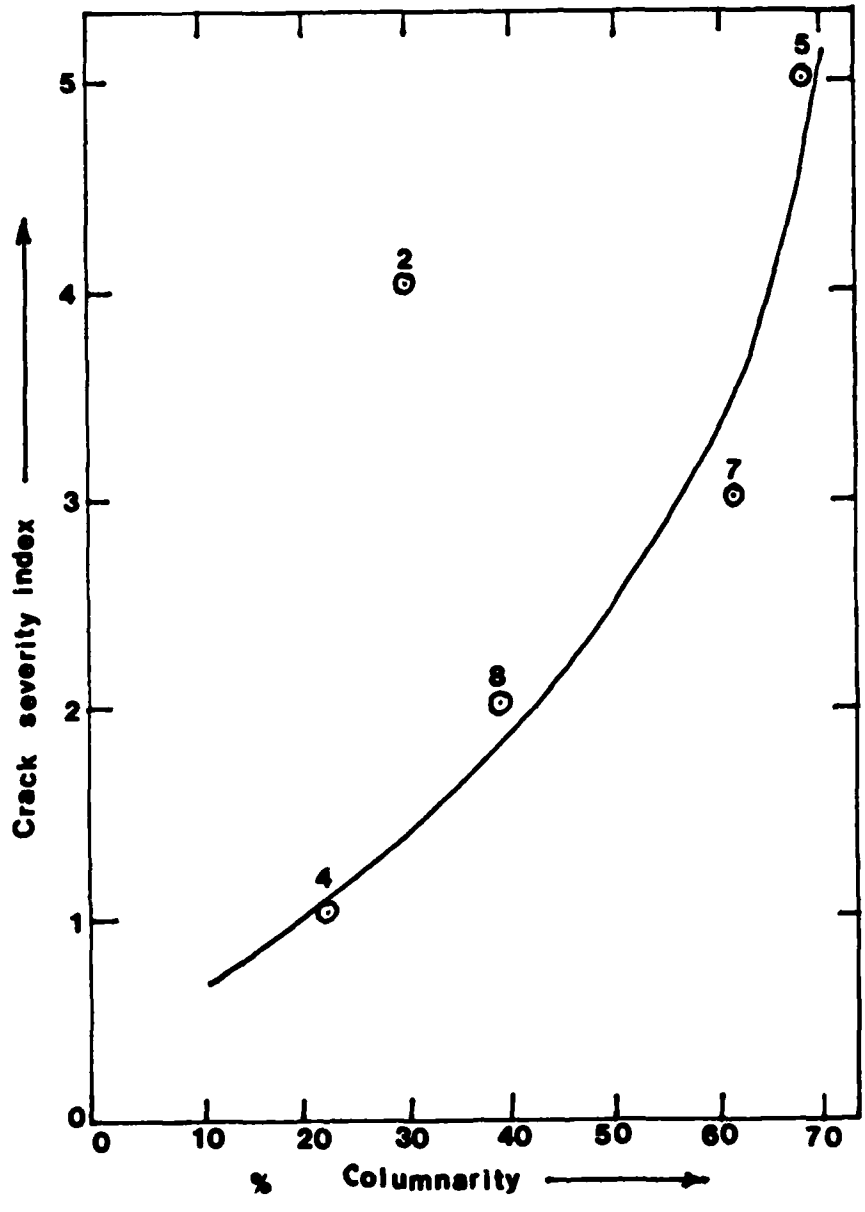

Figure 9: Effect of (surface) columnarity on the cracking severity during Varestraint test. Number of specimens considered is shown at every data point.

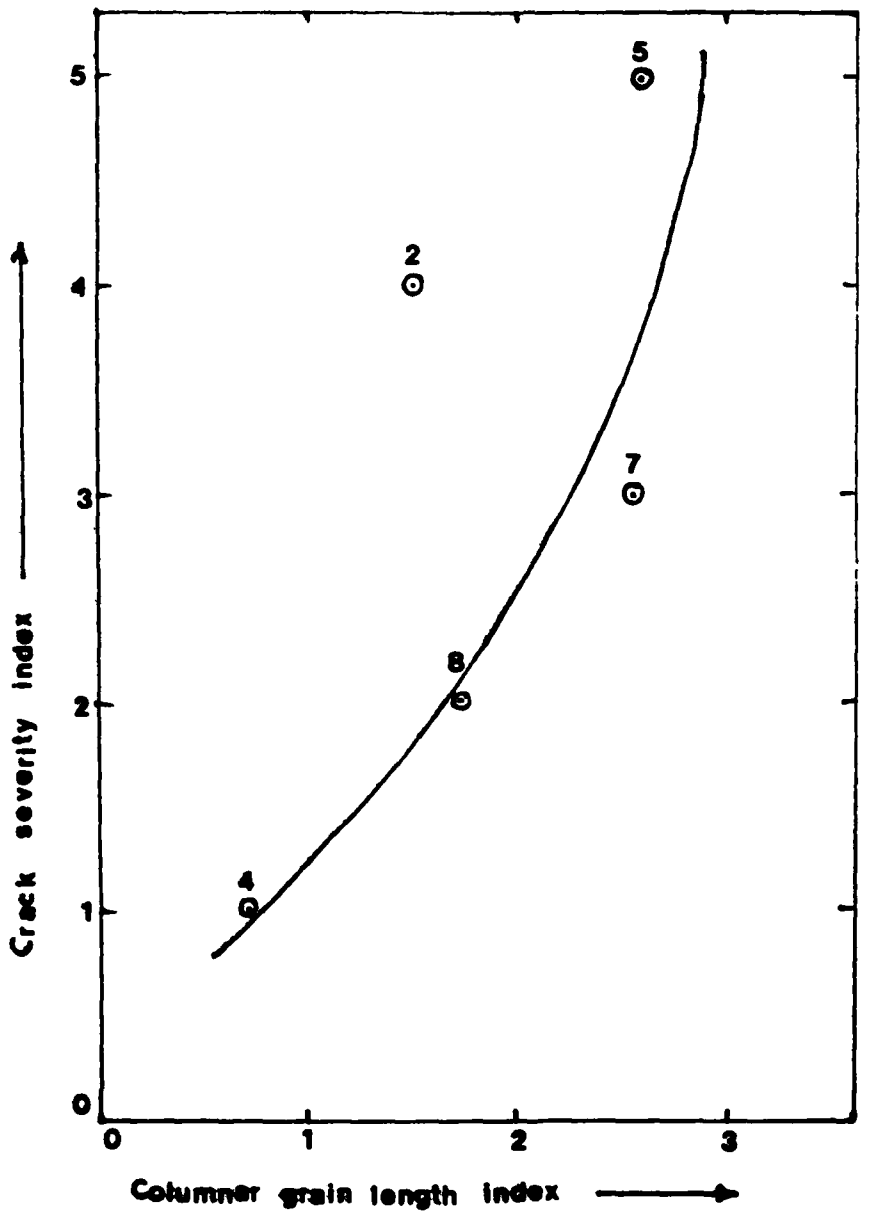

Figure 10: Variation of crack severity with columnar grain length. Number of specimens considered is shown at every data point.

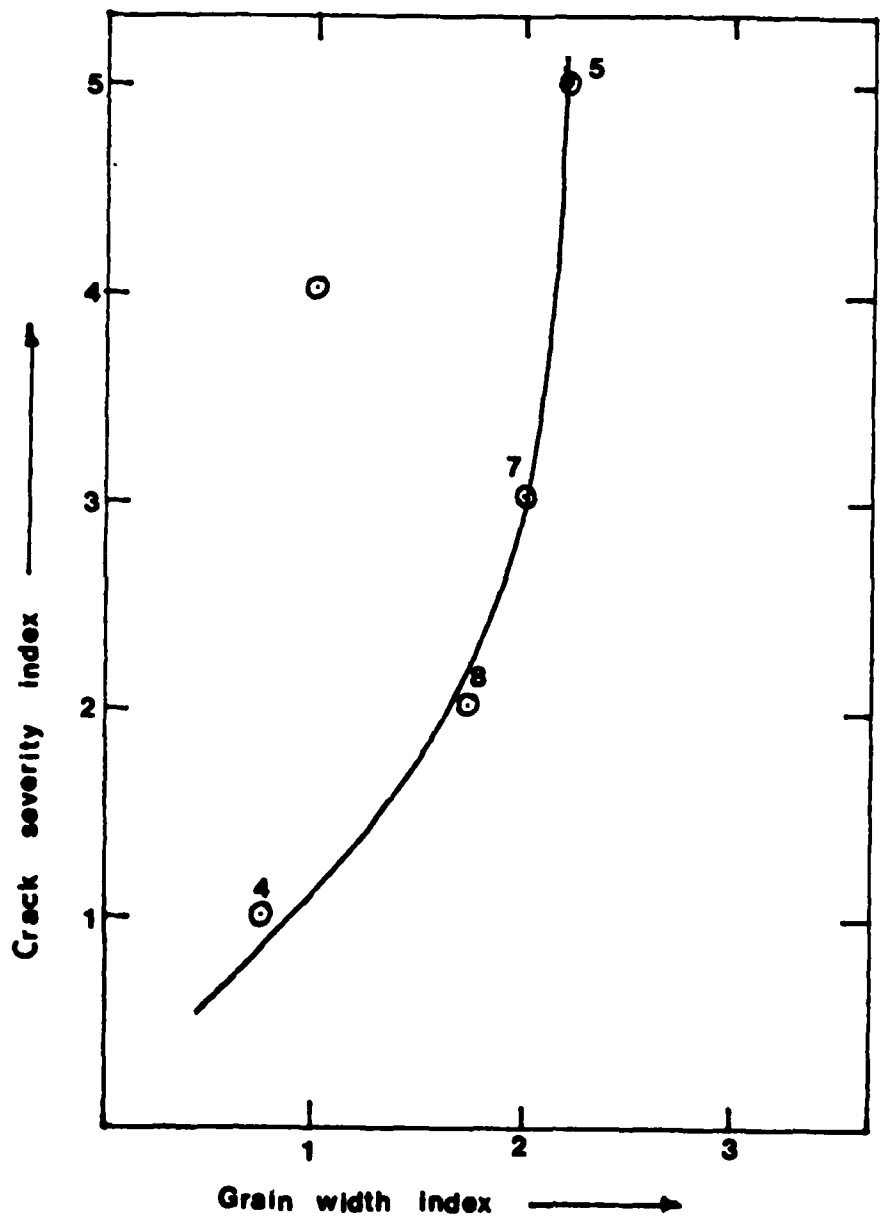

Figure 11: Effect of the width of columnar grains on the cracking severity during Varestraint test. Number of specimens considered is shown at each data point.

Figure 13: Microstructure of the weld zone in Specimen No. 2-9 (longitudinal cross section along the weld centerline). Apparent columnarity = 10-20%.

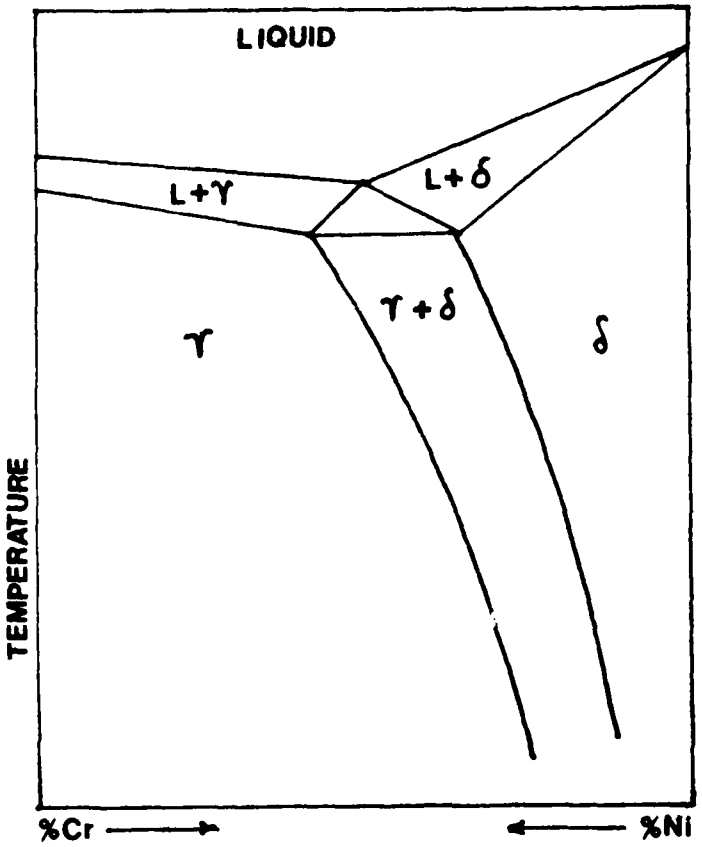

Figure 14: Generalized pseudo-binary diagram of stainless steel.

M
January 1978

SUPPLEMENTARY DISTRIBUTION LIST

Technical and Summary Reports

Professor G. S. Ansell
Rensselaer Polytechnic Institute
Dept. of Metallurgical Engineering
Troy, New York 12181

Professor H. K. Birnbaum
University of Illinois
Department of Metallurgy
Urbana, Illinois 61801

Dr. E. M. Breinan
United Aircraft Corporation
United Aircraft Res. Laboratories
East Hartford, Connecticut 06108

Professor H. D. Brody
University of Pittsburgh
School of Engineering
Pittsburgh, Pennsylvania 15261

Mr. P. J. Cacciatore
General Dynamics
Electric Boat Division
Eastern Point Road
Groton, Connecticut 06340

Professor J. B. Cohen
Northwestern University
Dept. of Material Sciences
Evanston, Illinois 60201

Professor M. Cohen
Massachusetts Institute of Technology
Department of Metallurgy
Cambridge, Massachusetts 02139

Professor Thomas W. Eagar
Massachusetts Institute of Technology
Department of Materials
Science and Engineering
Cambridge, Massachusetts 02139

Professor B. C. Giessen
Northeastern University
Department of Chemistry
Boston, Massachusetts 02115

Professor D. G. Howden
Ohio State University
Dept. of Welding Engineering
190 West 19th Avenue
Columbus, Ohio 43210

Dr. C. S. Kortovich
TRW, Inc.
23555 Euclid Avenue
Cleveland, Ohio 44117

Professor D. A. Koss
Michigan Technological University
College of Engineering
Houghton, Michigan 49931

Professor A. Lawley
Drexel University
Dept. of Metallurgical Engineering
Philadelphia, Pennsylvania 19104

Professor Harris Marcus
The University of Texas at Austin
College of Engineering
Austin, Texas 78712

Dr. H. Margolin
Polytechnic Institute of New York
333 Jay Street
Brooklyn, New York 11201

Professor K. Masubuchi
Massachusetts Institute of Technology
Department of Ocean Engineering
Cambridge, Massachusetts 02139

SUPPLEMENTARY DISTRIBUTION LIST (Cont'd)

Professor J. W. Morris, Jr.
University of California
College of Engineering
Berkeley, California 94720

Dr. Neil E. Paton
Rockwell International
Science Center
1049 Camino Dos Rios
P.O. Box 1085
Thousand Oaks, California 91360

Mr. A. Pollack
Naval Ships Research & Development
Center
Annapolis, Maryland 21402

Professor W. F. Savage
Rensselaer Polytechnic Institute
School of Engineering
Troy, New York 12181

Professor O. D. Sherby
Stanford University
Materials Sciences Division
Stanford, California 94300

Dr. Ronald DeYoung
David Taylor Naval Ship R&D Center
Code 1720.1
Bethesda, MD 20084

Dr. E. A. Starke, Jr.
Georgia Institute of Technology
School of Chemical Engineering
Atlanta, Georgia 30332

Professor David Turnbull
Harvard University
Division of Engineering and
Applied Physics
Cambridge, Massachusetts 02139

Dr. F. E. Wawner
University of Virginia
School of Engineering and Applied
Science
Charlottesville, Virginia 22901

Dr. C. R. Whitsett
McDonnell Douglas Research
McDonnell Douglas Corporation
Saint Louis, Missouri 63166

Dr. J. C. Williams
Carnegie-Mellon University
Department of Metallurgy and
Materials Sciences
Schenley Park
Pittsburgh, Pennsylvania 15213

Professor H. G. F. Wilsdorf
University of Virginia
Charlottesville, Virginia 22903

Dr. M. A. Wright
University of Tennessee
Space Institute
Tullahoma, Tennessee 37388

Elliott Company
Division of Carrier Corp.
Jeannette, PA 15644

Dr. B. MacDonald, Code 471
Chief of Naval Research
800 North Quincy St.
Arlington, VA 22217

BASIC DISTRIBUTION LIST

Technical and Summary Reports April 1978

Organization	Copies
Defense Documentation Center Cameron Station Alexandria, VA 22314	12
Office of Naval Research Department of the Navy 800 N. Quincy Street Arlington, VA 22217	
ATTN: Code 471	1
Code 102	1
Code 470	1
Commanding Officer Office of Naval Research Branch Office Building 114, Section D 666 Summer Street Boston, MA 02210	1
Commanding Officer Office of Naval Research Branch Office 536 South Clark Street Chicago, IL 60605	1
Office of Naval Research San Francisco Area Office 760 Market Street, Room 447 San Francisco, CA 94102	1
Naval Research Laboratory Washington, DC 20375	
ATTN: Codes 6000	1
6100	1
6300	1
6400	1
2627	1
Naval Air Development Center Code 302 Warminster, PA 18964 ATTN: Mr. F. S. Williams	1

Organization	Copies
Naval Air Propulsion Test Center Trenton, NJ 08628 ATTN: Library	1
Naval Construction Batallion Civil Engineering Laboratory Port Hueneme, CA 93043 ATTN: Materials Division	1
Naval Electronics Laboratory San Diego, CA 92152 ATTN: Electron Materials Sciences Division	1
Naval Missile Center Materials Consultant Code 3312-1 Point Mugu, CA 92041	1
Commanding Officer Naval Surface Weapons Center White Oak Laboratory Silver Spring, MD 20910 ATTN: Library	1
David W. Taylor Naval Ship Research and Development Center Materials Department Annapolis, MD 21402	1
Naval Undersea Center San Diego, CA 92132 ATTN: Library	1
Naval Underwater System Center Newport, RI 02840 ATTN: Library	1
Naval Weapons Center China Lake, CA 93555 ATTN: Library	1
Naval Postgraduate School Monterey, CA 93940 ATTN: Mechanical Engineering Department	1

BASIC DISTRIBUTION LIST (cont'd)

Organization	Copies
Naval Air Systems Command Washington, DC 20360 ATTN: Codes 52031 52032	1
Naval Sea System Command Washington, DC 20362 ATTN: Code 035	1
Naval Facilities Engineering Command Alexandria, VA 22331 ATTN: Code 03	1
Scientific Advisor Commandant of the Marine Corps Washington, DC 20380 ATTN: Code AX	1
Naval Ship Engineering Center Department of the Navy Washington, DC 20360 ATTN: Code 6101	1
Army Research Office P.O. Box 12211 Triangle Park, NC 27709 ATTN: Metallurgy & Ceramics Program	1
Army Materials and Mechanics Research Center Watertown, MA 02172 ATTN: Research Programs Office	1
Air Force Office of Scientific Research Bldg. 410 Bolling Air Force Base Washington, DC 20332 ATTN: Chemical Science Directorate	1
Electronics & Solid State Sciences Directorate	1
Air Force Materials Laboratory Wright-Patterson AFB Dayton, OH 45433	1
Library Building 50, Rm 134 Lawrence Radiation Laboratory Berkeley, CA	1

Organization	Copies
NASA Headquarters Washington, DC 20546 ATTN: Code RRM	1
NASA Lewis Research Center 21000 Brookpark Road Cleveland, OH 44135 ATTN: Library	1
National Bureau of Standards Washington, DC 20234 ATTN: Metallurgy Division	1
Inorganic Materials Div.	1
Director Applied Physics Laboratory University of Washington 1013 Northeast Forthieth Street Seattle, WA 98105	1
Defense Metals and Ceramics Information Center Battelle Memorial Institute 505 King Avenue Columbus, OH 43201	1
Metals and Ceramics Division Oak Ridge National Laboratory P.O. Box X Oak Ridge, TN 37380	1
Los Alamos Scientific Laboratory P.O. Box 1663 Los Alamos, NM 87544 ATTN: Report Librarian	1
Argonne National Laboratory Metallurgy Division P.O. Box 229 Lemont, IL 60439	1
Brookhaven National Laboratory Technical Information Division Upton, Long Island New York 11973 ATTN: Research Library	1
Office of Naval Research Branch Office 1030 East Green Street Pasadena, CA 91106	1